7-19-2023

The effect of heating area and Wheatstone bridge materials on a thermally actuated MEMS viscosity sensor

Connor Michael Levine
cxl4088@rit.edu

The effect of heating area and Wheatstone bridge materials on a thermally actuated MEMS viscosity sensor

by

Connor Michael Levine

Thesis

Submitted in Partial Fulfillment of the Requirements for the Degree of

MASTER OF SCIENCE IN ELECTRICAL ENGINEERING

Department of Electrical and Microelectronic Engineering

Kate Gleason College of Engineering

Rochester Institute of Technology, Rochester, NY

Supervised by:

Dr. Ivan Puchades

July 19, 2023

The effect of heating area and Wheatstone bridge materials on a thermally actuated MEMS viscosity sensor

Approved by:

Thesis Primary Advisor: Dr. Ivan Puchades Date

Committee Member: Dr. Karl Hirschman Date

Committee Member: Dr. Robert Pearson Date

Department Head: Dr. Ferat Sahin Date

Acknowledgements

I would like to thank my family for supporting me throughout my academic career. My parents Glenn and Kelly and my brother and sister Aidan and Kaitlin. Without your help I would not have made it to where I am today. I owe my success to you all of you pushing me to be the best I can.

I would also like to thank Dr. Ivan Puchades for advising me throughout this project. And for also teaching me the fundamentals of MEMS. You gave me the freedom to pursue this project how I wanted but was also always there to help with any problems that's I ran into.

I would also like to thank the fellow members of my research group for assisting me throughout this project from teaching me how to run equipment in the clean room to assisting with data collection: Amough, Lukas, Will and Chris.

Thank you to Poseidon Systems and the Nano Power Research Labs for funding this project. Without their help this project would not have been possible.

I would like to also thank the staff of the Electrical and Microelectronic engineering department for providing the resources and equipment used in this project.

Abstract

Being able to accurately measure oil viscosity in real time is critical for multiple applications. It can ensure that the oil being used to protect and lubricate gears and other mechanical elements is good. To do this a thermally actuated micro electromechanical systems (MEMS) based sensor has been previously developed. The sensor is able to measure viscosity by having the fluid couple with the oscillating diaphragm and monitoring the frequency, amplitude and quality factor of the waveform. To improve the accuracy of the sensor, 5 different versions were created to study the effects of heating area and the sensing material used in the Wheatstone bridge. To also improve the repeatability of the sensors and reduce sensor to sensor variation the fabrication process was improved. This included the use of SOI wafers and better diaphragm alignment through the use of a contact aligner with an IR attachment to show alignment marks through the wafer. For the Wheatstone bridge polysilicon and P+ diffusion resistors were evaluated. For the heater material polysilicon and P+ diffusion were evaluated. For the heater area 3 separate designs were made with different size polysilicon heaters but with the same P+ Wheatstone stone to allow just the heater size to be evaluated. To remove the effects of temperature on the sensors each sensor was run through a temperature sweep in air. The data was used to create a correction factor that applied to the fast Fourier transform (FFT) frequency to produce more accurate results for measurements taken above room temperature. To determine how sensitive each type was to changes in viscosity each type was placed in N100, N35 and N10 oils while their temperature went from 25°C to 80°C. These oils were used because they made specific ASTM standards to ensure they have a set viscosity for a given temperature. From testing it was determined that higher initial deflection of the diaphragm does not equate to a higher sensitivity.

TABLE OF CONTENTS

Table of Figures

Table of tables

Introduction

It is important to get an accurate reading of an oil's viscosity to ensure components are being properly protected in a system. This is especially critical for engines, gear boxes, transmissions as the oil is there to protect the gears and prevent them from being worn excessively. The viscosity of an oil will change as it continues to run through a system, this can be caused by absorbing moisture, contaminates building up in lines and the oil breaking down from wear. A study showed that an increased kinematic viscosity can be caused by increased oxidation which can make it harder for gears to spin. While the kinematic viscosity can be decreased due to oil shear, [1] causing decreased protection from wear.

In order to monitor the health of the oil and determine when it's time to change the oil, viscosity can be monitored in real time. This allows the system to determine when it's time to change the oil. Instead of relying on an engine time or a mileage standard, which can lead to oil being changed later than is should be when it already past its minimum health. It can also be changed earlier than needed when plenty of life still remains adding an increased maintenance cost. By monitoring viscosity in real time oil can be changed to oil when it needs to, providing an additional cost-saving measure by helping to reduce wear on equipment.

Monitoring just the viscosity in real time is not enough to gauge an oil's health alone. Viscosity is also dependent on temperature. As temperature increases viscosity will decrease. Because of this when a system such an engine first starts the oil will cold and have a higher viscosity than when it reaches operating temperature. A temperature change of a few degrees can change the viscosity of the oil a few centistokes requiring an accurate sensor. To ensure an accurate viscosity reading for the current system conditions temperature must also be monitored in real time.

The goal of this project is to study the effect of heating area and sensing materials of a thermally actuated MEMS viscosity sensor to maximize sensitivity. To accomplish this, 5 different versions of varying heater sizes and Wheatstone bridge materials were created. This studies the effect of 3 different sizes heater and two different Wheatstone bridge materials. By fulling characterizing and evaluating each sensor type in different oil viscosities ranging from water like to very viscous viscosity ranges of each type will be determined. The sensor will also be tested in

temperatures ranging from 23°C to 80°C to simulate real world operating conditions to determine which sensor will operate the best for a variety of conditions.

Literature Review

2.1 Viscosity Fundamentals

Viscosity is a measure of a fluid's resistance to flow. It can be broken into two categories Dynamic viscosity and Kinematic viscosity. Dynamic viscosity can be defined as a fluid's resistance to flow under an external force. Kinematic viscosity is the fluids resistance to flow under gravitational forces. [2] Kinematic viscosity is measured in Stokes (St) which is equivalent to 10^{-4} m^2/s. Most measurements are in centistokes (cSt) for easy of measurements 1 St = 100 cSt. To have a refence on how viscous a centistoke is water is 1 cSt while a thicker fluid such as syrup can be up to 1,000 cSt. Figure 1 shows the difference between high and low viscosity.

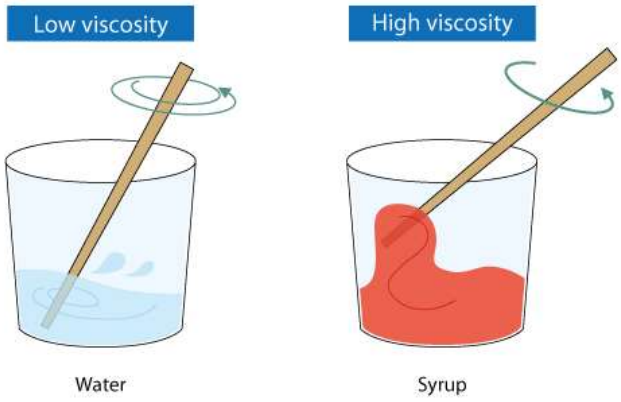

Figure 1 Illustration of viscosity

Viscosity is an important measurement in multiple fields ranging from the automotive to medical sectors. This is because viscosity can be used as a way of determining a fluid's health. For example, the engine oil in a car will be a set viscosity when it is first put in, however after running for hundreds of hours contaminates can start to build up. These will reduce the oils' ability to protect the engine and cause increased ware on components. As the amount of contamination increases the oil's viscosity will change. By monitoring the change in viscosity, it

can be determined when to change the oil. Figure 2 shows the difference between a clean sample of 10W30 and contaminated 10W30. The contaminated sample has a higher viscosity than the clean sample.

Figure 2 Clean 10W30(left) and contaminated 10W30 (Right)

2.2 Ways of measuring viscosity

Viscosity can be measured in serval ways with the proper lab setup. One common way of measuring viscosity is the Capillary viscometer method shown in Figure 3. First oil is drawn into the tube with suction up till the starting mark. Next the suction is removed the fluid is timed by how long it takes to move from the starting mark to the ending mark. Based on the time it takes the fluid to move viscosity can be calculated.

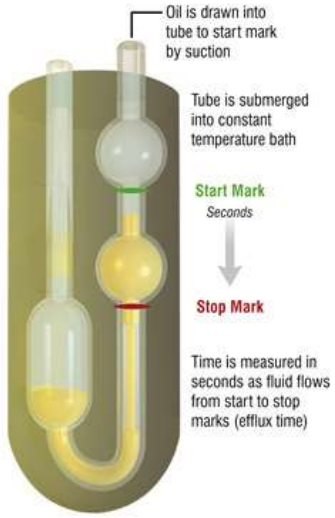

Figure 3 Capillary viscometer

Another common method is the rotational viscometer Figure 4. It submerges a spindle into the fluid and then rotates it. It is then able to determine viscosity based on the amount of torque required to rotate the spindle at a set speed [3].

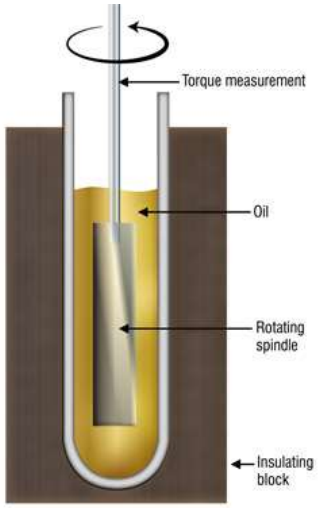

Figure 4 Rotational Viscometer

These methods allow for reliable viscosity measurements and are the typical ASTM standards for measuring viscosity. However, these methods do not allow for real time measurements outside of a laboratory, due to requiring large and bulky equipment.

2.3 MEMS viscosity sensors

There are currently a few types of MEMS based viscosity sensors and few are widely available for purchase or used in industry. They are broken into a few main modes of operation, capillary based, ultrasonic transducers, cantilever structures and piezoelectric resonators. The most common type is the cantilever which operates by having oscillating beam submerged in the fluid. These oscillations are then monitored in real time as they will change as viscosity changes.

2.4 Temperature effect on viscosity

Viscosity is dependent on temperature, as temperature increases the viscosity of a fluid will decrease. However, the change in viscosity is not fully linear, As shown in Figure 5

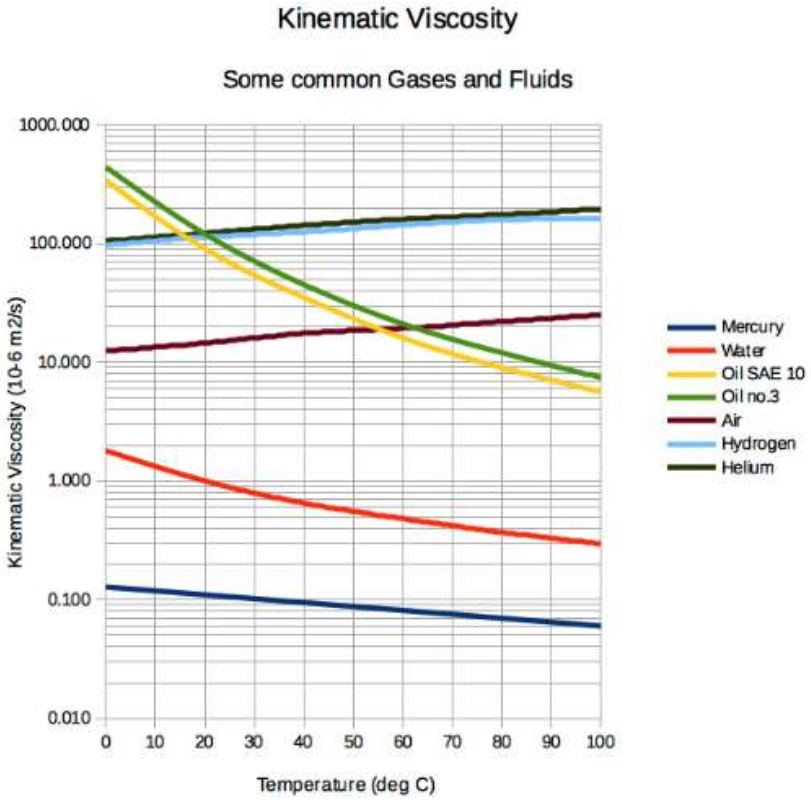

Figure 5 Temperature effects on kinematic viscosity

Because temperature heavily affects viscosity measurements, temperature must be monitored and maintained during the measurement process. Depending on the fluid being measured a fluctuation of a couple of degrees can produce very different results. For example, a sample of

N100 oil at 20°C has a kinematic viscosity of 320.5 cSt while at 25°C it is 230.5 cSt [4]. A difference of 5°C causes a change of 100 cSt. While not all oils have this large of a change its important to actively monitor the temperature of the fluid to ensure a proper viscosity measurement is taken. This is especially important for many real-world applications such as the engine oil used in a car. If the car has been sitting off for a while the oil will cold and have a higher viscosity when the car first starts as opposed to if the car has been running for a while. If the viscosity of the oil was taken right as the car started before it warmed up with a temperature reading it would be consisted out of spec. However, if the temperature was also being actively monitored along with viscosity, then it would show that the oil is at an acceptable viscosity. To help deal with the problem the proposed viscosity sensor will have a built-in temperature sensor to actively correlate viscosity measurements.

Thermally actuated MEMS viscosity sensor

Operating principle

The sensor works on the principle of having an oscillating diaphragm that will couple with the fluid being measured changing its frequency and amplitude of oscillation. This can then be correlated to viscosity by recording the output of the sensor at a known oil viscosity value.

3.2 Diaphragm oscillations and resonance

To create the oscillations a heating resistor in embedded in the diaphragm, voltage is applied to the heater for a fraction of a second which is enough to heat the diaphragm up causing it to expand upwards as shown in Figure 6B. Once the voltage is removed the diaphragm quickly cools and returns to its original shape. However, the excess energy causes the diaphragm to oscillate shown in Figure 6C.

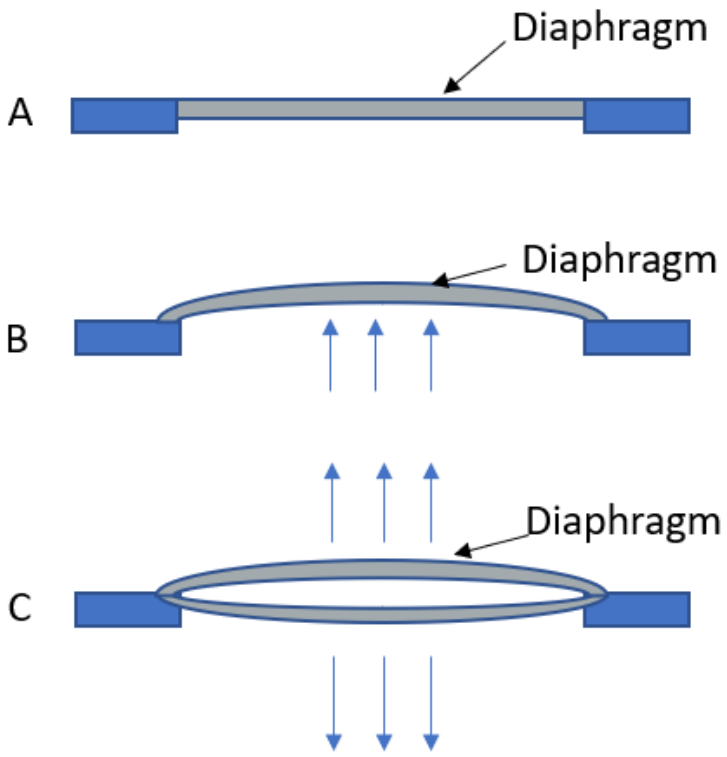

Figure 6 Diaphragm deflection

These oscillations are then detected by the pizeoresistors embedded in the diaphragm as voltage changes from the output of a Wheatstone bridge. The changes are then used to determine its frequency, amplitude, and quality factor of the oscillations. When the diaphragm is submerged in a fluid its frequency will decrease. This will also cause the amplitude and quality factor of the waveform to decrease. The more viscous a fluid is the lower its frequency will be as the oscillations become more heavily damped. The Frequency will increase when submerged in a thinner oil as the oscillations will be less damped however it will still oscillate a lower frequency than if it was in air. Using this principle, the viscosity of a fluid can be determined.

The natural frequency of the sensor can be calculated by using the equation (1) [5]

$$Frequecny_{air} = \frac{19.74}{2\pi a^2}\left[\frac{Eh^3}{12\rho h(1-\nu^2)}\right]^{1/2} \qquad (1)$$

Where E is the Youngs modulus of silicon, a is length of the plate, h is the thickness of the diaphragm ρ is density and ν is Poisson ratio. For silicon the Youngs modules is 190 GPA, the density is 2330 kg/m^3.Uisng a diaphragm thickness of 15 μm and a length of 2.5 mm, in air the diaphragm will oscillate at 20 kHz. However, the actual frequency of each sensor will vary slightly as there are minor deviations in diaphragm thickness across the wafers.

The change in frequency due to the diaphragm coupling with the fluid being measured can be calculated using the following formula:

$$\omega_{fluid} = \frac{\omega_{vacuum}}{\sqrt{1+\beta}} \quad (2)$$

Where ω_{fluid} is the angular frequency of diaphragm while submersed in the fluid, ω_{vacumm} is the angular frequency outside of fluid β is virtual mass added by the fluid. [6]

The virtual mass β can be calculated as follows where ρ_{fluid} is density of the fluid and ρ_{plate} is the density of the plate.

$$\beta = 0.669 \frac{\rho_{fluid} a}{\rho_{plate} h} \quad (3)$$

The radius of the plate is a, the thickness of plate is h. These formulas are designed for circular plate however they can be used to estimate the change in frequency for the rectangular plate.

3.4 Pizeoresistor material used in the Wheatstone bridge

Different materials have varying piezoresistive coefficients which will determine how much the resistance will change based on the amount of stress applied. The materials chosen for use in the Wheatstone bridge as the piezoresistive strain gauges are polysilicon and P+ diffusion regions. These materials differ in a few keyways. P+ is a heavily doped region of silicon. In the case of this project, it's heavily doped with boron through ion implantation. Boron is used because it has one less valance electron than silicon and allows it to substitute for a silicon atom. Because it is missing an electron it can't bond with any surrounding silicon atoms. This creates an electron hole and since it's a heavily doped area it becomes a region with a high connection of holes. Due to the N-type wafers chosen for fabrications the P+ regions will create a P-N junction

[7]. Because it forms a P-N junction it will have a lower heat resistance than polysilicon. As the temperature increases the junction will progressively break down due to an increased number of free carriers.

Polysilicon differs from P+ resistors in that instead of becoming part of the silicon lattice of the wafer it makes the resistors as its own region. Polysilicon is made up of many small silicon crystals. Polysilicon pizeoresistors are made by depositing a layer of polysilicon through low-pressure Chemical Vapor Deposition (LPCVD)The resistance of the polysilicon will also depend on temperature and can be calculated using the formula for the Temperature Coefficient of Resistance (TCR) (4) [8]

$$TCR = \left(\frac{1}{R}\right)\left(\frac{\partial R}{\partial T}\right) \quad (4)$$

Where R is the resistance, ∂R is the change in resistance and ∂T is the change in temperature. Due to this it's able to withstand higher temperatures when compared to P+ resistors. However due to its lower piezo resistive coefficient it will produce a smaller output.

The expected change in resistance due to stain can be calculated by

$$G = \frac{\Delta R}{\frac{R}{\varepsilon}} \quad (5)$$

From the equation G is the gauge factor, R is the resistance and ε is the strain. As the diaphragm oscillates it will cause the pizeoresistors to expand and shrink in size. This will result in a resistance that can be monitored by observing the change in voltage from each side of the Wheatstone bridge. The two outputs are then used to create the sole output of the bridge that results in an oscillating waveform representing the operation of the diaphragm.

With our Process at RIT, we can target a resistance of 40 Ω/Sq for polysilicon, while for P+ we can target 110 Ω/Sq. This also accounts for how much the resistance will change due to strain because P+ has a higher resistance it will result in a higher change.

3.5 Heater size and material

The size of the heater will affect how much the diaphragm will deflect along with how much power it will require. To determine the impact of heater size on amount of diaphragm deflection and power required a first order approximation was done. Because of this the radius of a square was chosen to allow the formula to still be used.

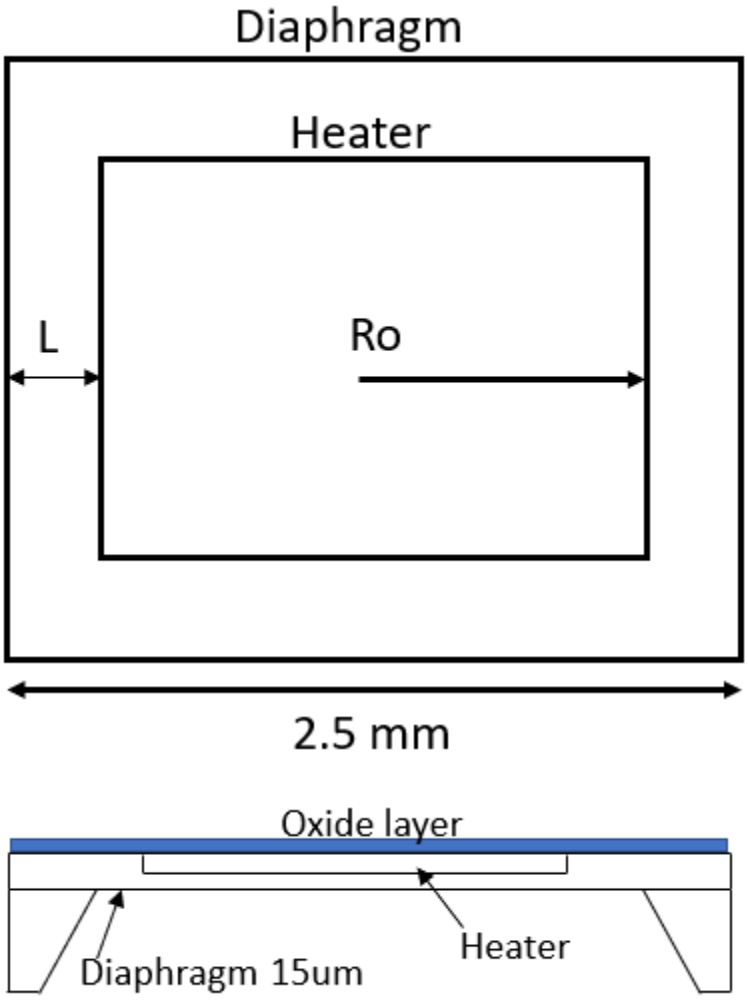

Figure 7 Heater size approximation

Using the set size of the diaphragm three separate heaters sizes were chosen.

$$R_{th} = \frac{1}{C} * \frac{L}{A} \qquad (5)$$

Where C is the thermal conductivity (W/mK) L is the thermal path from the heater to the diaphragm (m) and A is the cross-sectional area (m^2).

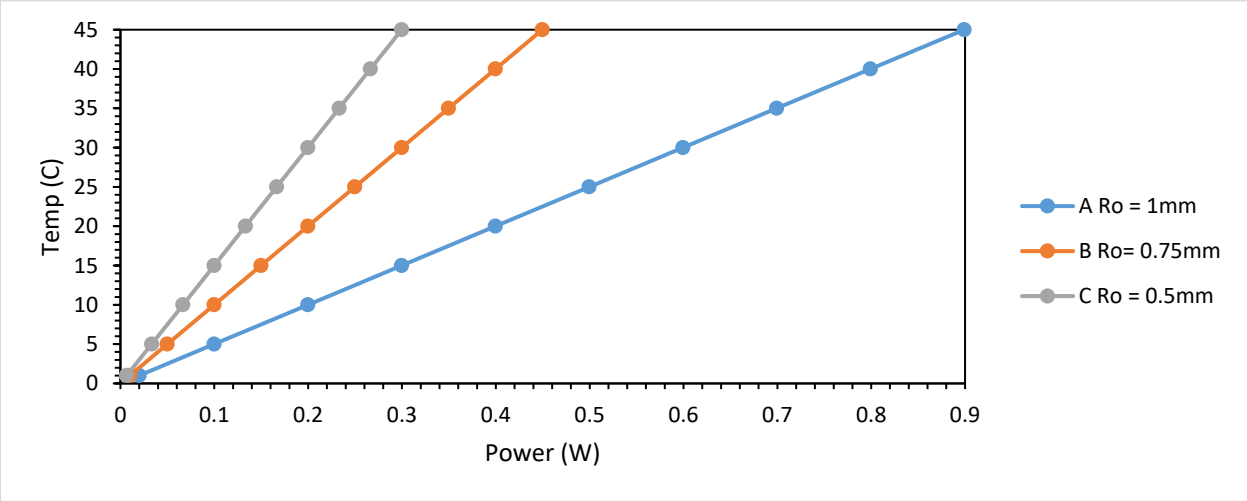

Figure 8 Temperature of heater vs Power applied.

From the calculations (Figure 8) the smaller heater (0.5 mm) was able to reach at higher temperature at lower power setting when compared to the large heater (1 mm). By having a higher temperature change at lower power setting, this will allow the sensor with the smallest heater to operate on less power. This can be critical for application where power is limited.

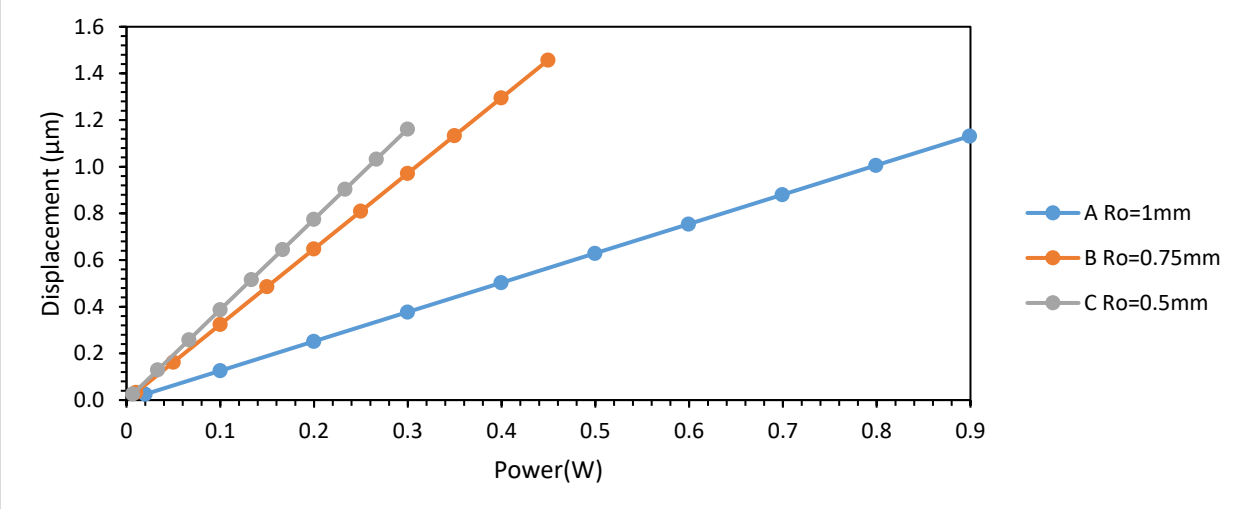

Figure 9 Predicted displacement of diaphragm vs power.

Due to the higher temperatures the smaller heater will also be able to reach a large initial displacement at lower power settings (Figure 9). This will allow for a potentially larger signal from the Wheatstone bridge as the piezo resistor will experience higher strain. At 0.3 W the 0.5mm heater will displace 1.1 µm. The 0.75 mmm heater will be able to displace 1.0 µm at 0.3W and the largest heater 1mm will displace only 0.4 µm at 0.3 W. The difference between the smallest and largest heater is 0.7 µm at 0.3 W for the 1mm heater to reach the same amount of displacement it will need to operate at 0.8 W which is 0.5 W higher.

Design of sensor types

The size of the heater along with the construction of the Wheatstone bridge will affect how the sensor operates. To determine the effect of each variable on the operation of the sensor. 5 different sensor types were made. Type 1 and 2 will use the same size polysilicon heater but different materials for the Wheatstone bridge to determine its effect on sensitivity. Type 3 will use the same bridge as type 2 however it will use a P+ heater to determine its effects. Type 4 and Type 5 will use two different size heaters but the same bridge as type 2 to measure the effect of heater size. Using the data collected from each fabricated sensor the optimum sensor configuration could be determined. All sensors will have a polysilicon resistor to be used as a temperature sensor. This was added to monitor the temperature of the fluid that the sensor is measuring. It is placed outside of the diaphragm region to prevent its resistance from changing due to strain of the diaphragm oscillating.

4.1 Type 1 Sensors

The type 1 sensor uses both a polysilicon heater and resistor. Its design is show in Figure 10 This version was created to allow the sensor to withstand higher temperatures. However, because it uses polysilicon for the Wheatstone bridge it will have lower sensitivity due to the material piezo resistive coefficient. It has a 2.5x2.5 mm diaphragm in the center with a heater that is 1.2x1.6 mm. It also has a polysilicon resistor to be used as a temperature sensor with a target resistance of 280 Ω. The Wheatstone bridge has a targeted resistance of 800 Ω while the heater has a targeted resistance of 200 Ω.

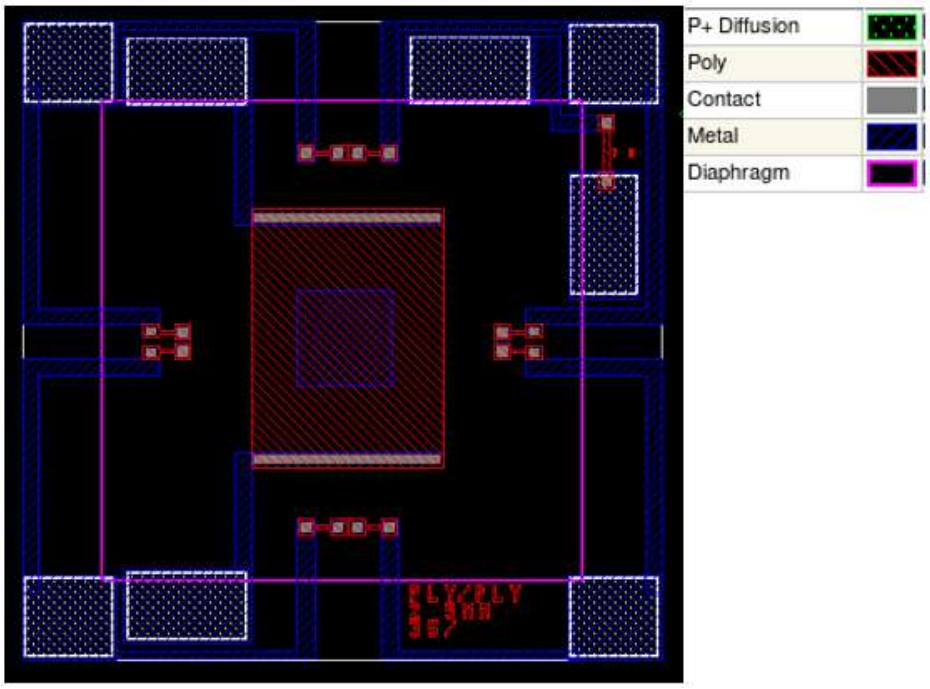

Figure 10 Type 1 sensor Layout

4.2 Type 2 Sensor

The type 2 sensor shown in Figure 11 uses the same polysilicon 1.2x1.6 mm heater as type 1 however it uses a different material for the Wheatstone bridge. Instead of polysilicon for the Wheatstone bridge it uses P+. This allows the bridge to be more sensitive to defections of the diaphragm allowing it to be more accurate when compared to the polysilicon. The Wheatstone bridge has a target resistance of 2000 Ω. However, because it uses P+ it won't be able to operate in the higher temperatures that Type 1 can.

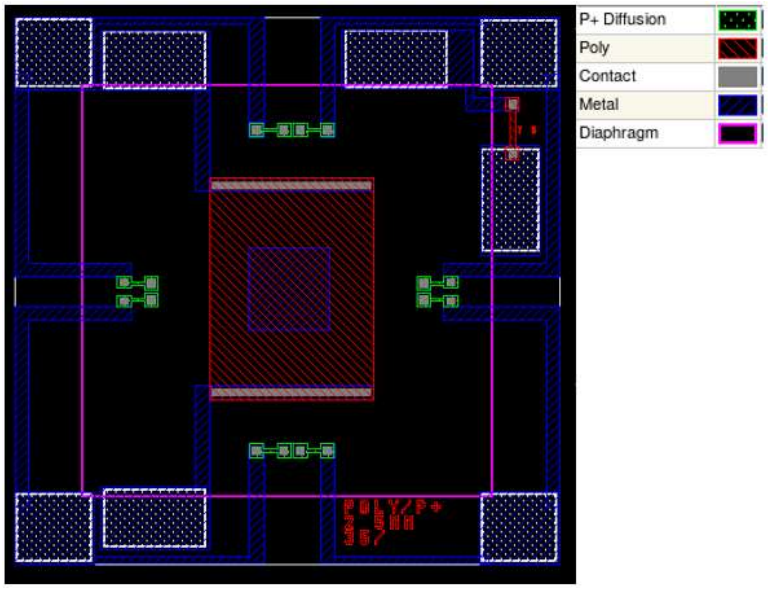

Figure 11 Type 2 Sensor Layout

4.3 Type 3 sensor

Type shown in Figure 12 uses a 1.2x1.6 mm heater that is made out of P+ with a targeted resistance of 150 Ω. It takes up approximately 35% of the area of the diaphragm. It also uses P+ for the Wheatstone bridge resistors. The bridge has a targeted resistance of 2000 Ω. This sensor is designed to test the effectiveness of P+ as the heater material and will be compared to Type 2 since they have the same Wheatstone bridge.

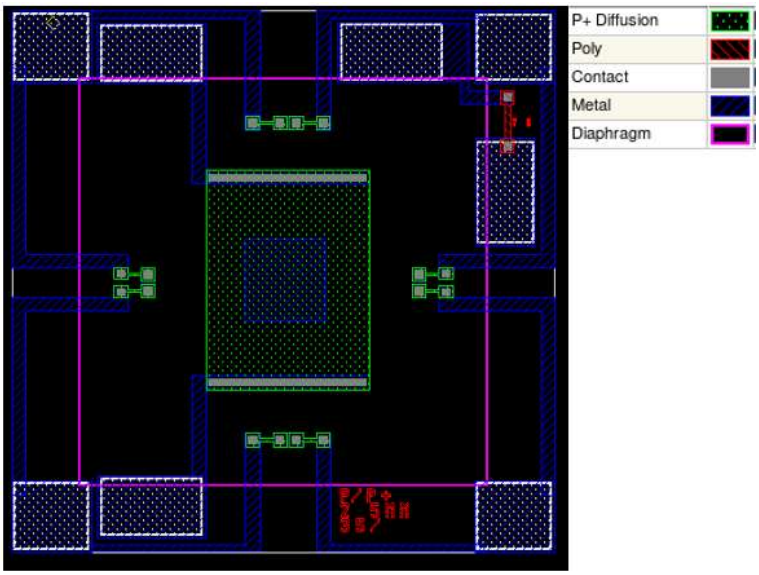

Figure 12 Type 3 Sensor Layout

4.4 Type 4 sensor

Type 4 shown in Figure 13 uses P+ Wheatstone bridge resistor and a polysilicon heater. This type is different from the previous designs by having a smaller heater. This heater is 0.8x1.3 mm which is 16% of the area of the diaphragm. Due to the smaller size of the heater, it should be able to operate at lower voltages than the previous types while providing a similar about of initial deflection. It has the same 2000 Ω P+ Wheatstone bridge as Type 2.

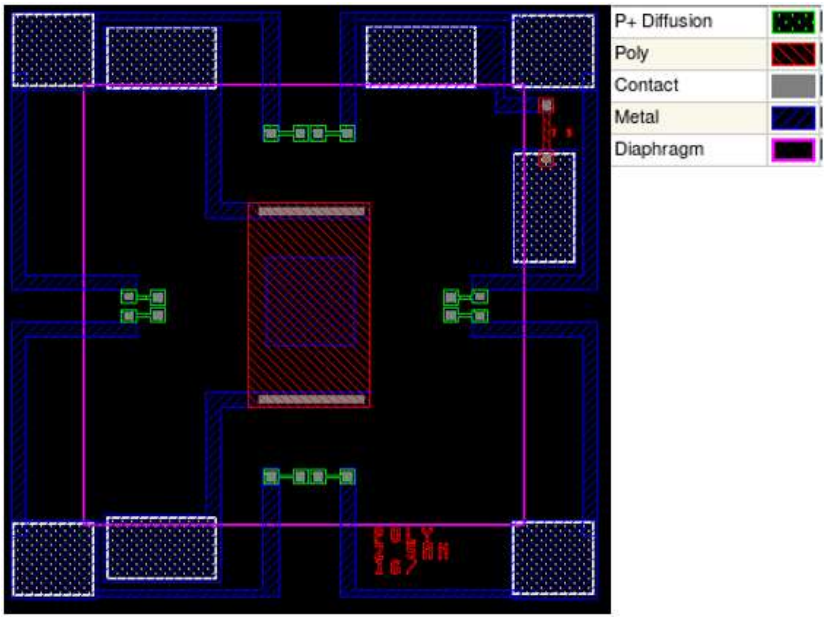

Figure 13 Type 4 Sensor layout

4.5 Type 5 sensor

Type 5 shown in Figure 14 uses P+ for the Wheatstone bridge but has the smallest polysilicon heater. This heater is 0.29x0.55 mm, it takes up 2% of the area of the diaphragm. This sensor is predicted to return the highest changes in amplitude measurements due to the diaphragm deflecting more at a lower power than types 1 through 4. It has the same 2000 Ω P+ Wheatstone bridge as Type 2.

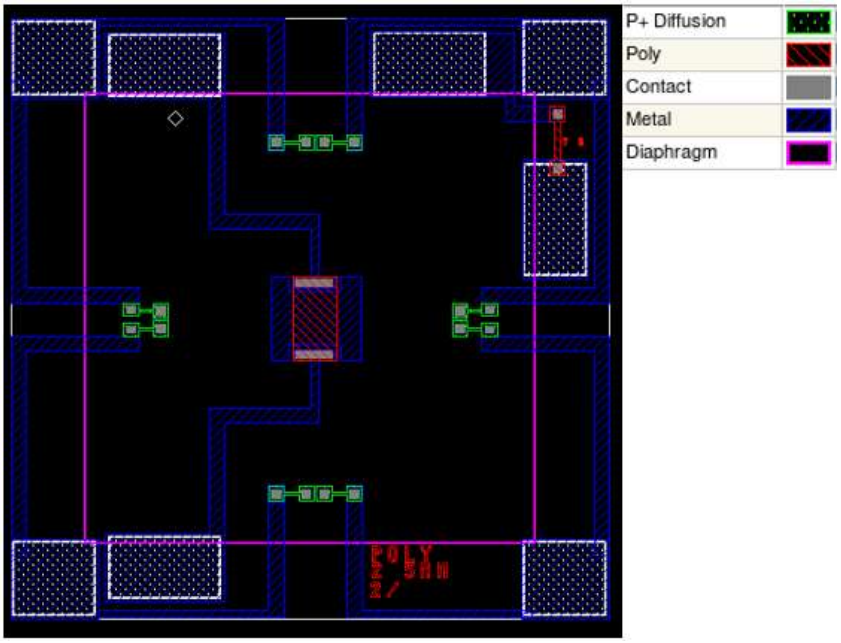

Figure 14 Type 5 sensor layout

Fabrication of sensors

Sensors were fabricated at RIT's Semiconductor and Microsystems Fabrication Laboratory. Production starts with 4" n-type <100> 500-550 µm silicon wafers. First an RCA clean was performed to remove any potential contamination before starting production. After cleaning a 6500 Å thermally grown masking oxide was grown over the wafer. After the oxide is grown, Photolithography is done to define the P+ implant regions. The standard photolithography process that is repeated throughout production is as follows. Before applying the photoresist, the wafers undergo an HMDS (hexamethyldisilizane) [9] process to improve adhesion. The MiR701 photoresist is applied using a CEE Spin station at 4000 rpm for 30 seconds. After coating the wafer is soft baked at 95 °C for 60 seconds. The photoresist is then exposed using the Karl Suss MA150 aligner with an i-line filter for 140 seconds. Next the photoresist is then developed using a CEE Spin developer. The wafers are then hard baked at 110°C for 60 seconds with the lithography step complete the oxide can now be etched. The oxide is wet etched using 10:1 BOE (Buffered oxide etch) opening up the P+ regions for implant as shown in Figure 15. With an etch rate of about 500 Å/Min the process takes 18 minutes to etch trough the oxide and open up the P+ regions.

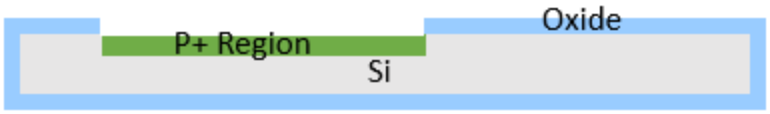

Figure 15 Oxide growth and definition of P+ region

The P+ region is then created by ion implantation of B11 at 45 keV. After implantation the photoresist is stripped off using a solvent strip process. Next a dopant diffusion process and 4000 Å wetox oxide is grown. Next a 1500Å nitride is deposited using an LPCVD. The oxide and nitride layers are shown in Figure 16.

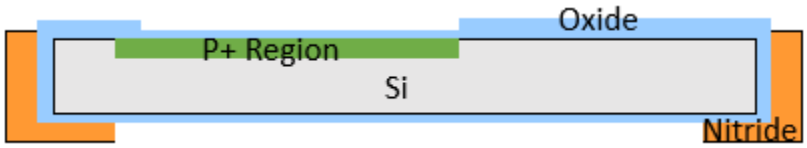

Figure 16 Nitride Growth and definition of backside diaphragm

After the nitride deposition the diaphragms on the backside are defined by performing the back side diaphragm lithography step. The nitride is then etched off the backside in 10:1 BOE. Next the Nitride is plasma etched off the front side of the wafer to remove it. After the nitride is removed from the front of the wafer the remaining oxide on the backside is etched in 10:1 BOE to open up the diaphragm regions. After the etch, the photoresist is solvent striped, and the wafer undergoes an RCA clean process with a 60 second dip in 50:1 HF after SC1. 6000 Å of poly is deposited by LCPVD, followed by an ion implant of polysilicon of P31. The poly is then diffused in nitrogen gas for 15 minutes at 1000°C. With the poly diffused the Poly layer lithography is done to define the poly regions on the front side of the wafer. The ploy is then plasma etched in a LAM490 to create the ploy pattern as shown in Figure 17.

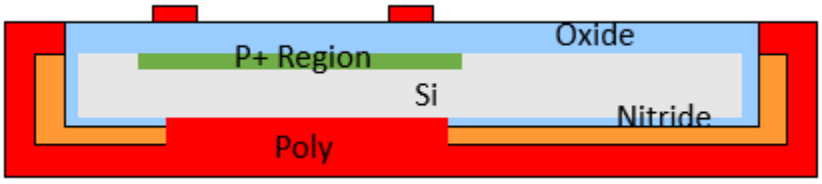

Figure 17 Polysilicon deposition and patterning

The photoresist is then solvent striped and another RCA clean is performed. 1µm of TEOS (Tetraethyl Orthosilicate**)** is then deposited on the wafer using the P5000. Next the contact cut lithography step is performed to define the contact cut regions. The contact cuts are etched in 10:1 BOE, the etch rate of TEOS was ~1000 Å/min while the oxide was etched at ~500 Å/ minute. The resulting cross section is shown in Figure 18.

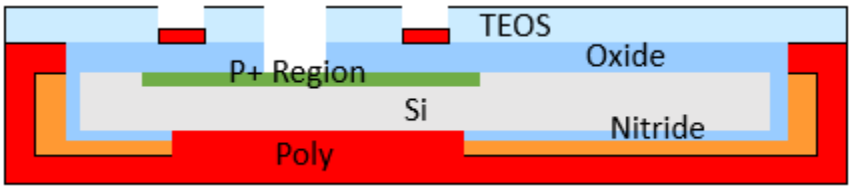

Figure 18 Dielectric deposition and contact cut.

After the contact cuts were verified by microscope inspection the photoresist was stripped and an RCA clean was performed. With the wafers clean and the contact cuts open 10,000 Å of aluminum is deposited using a glass jar thermal evaporator. With the aluminum deposited the metal lithography step can be performed. The metal is patterned and then wet etched for 6 minutes. Next it undergoes a freckle etch for 1 minute to remove any silicon residue. The resist is then solvent stiped and another 1 µm of TEOS is deposited as a passivation layer. The passivation layer lithography is performed to pattern the TEOS to create an opening for the metal contact pads. The TEOS is then etched in Pad etch. Then the photoresist is striped, and the resulting cross section is shown in Figure 19.

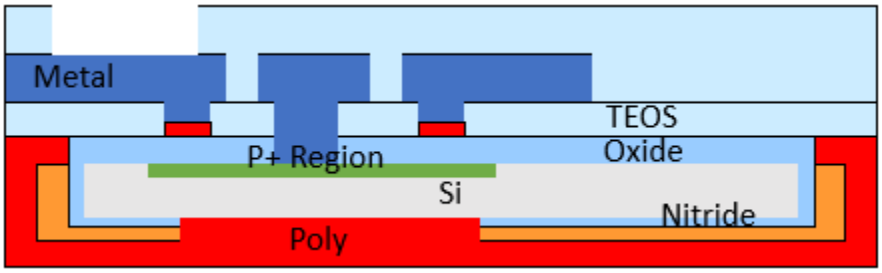

Figure 19 Metal deposition and patterning

To protect the front side of the wafer during the diaphragm etch ProTEK [10] is spin coated on the front side. With the frontside protected the diaphragm is etched in KOH (Potassium hydroxide) for 4 hours due to slow etch rate. To track the progress of the etch and

determine the time reaming to prevent over etching the wafers are periodically inspected under a microscope. The resulting structure after the diaphragm etch is shown in Figure 20.

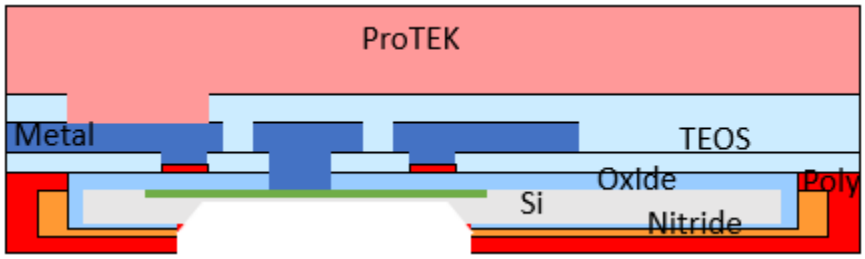

Figure 20 Diaphragm Etch

Once the etch is completed the ProTEK is striped off. The wafers undergo a final electrical test before dicing. After the wafers pass the electrical testing, the wafers are diced on a wafer saw to produce the individual die.

5.2 Fabricated devices

From production 5 different types of the sensor were made Figure 21 shows one fabricated sensors type 1 and type 2 sensors from lot 3 wafer P1

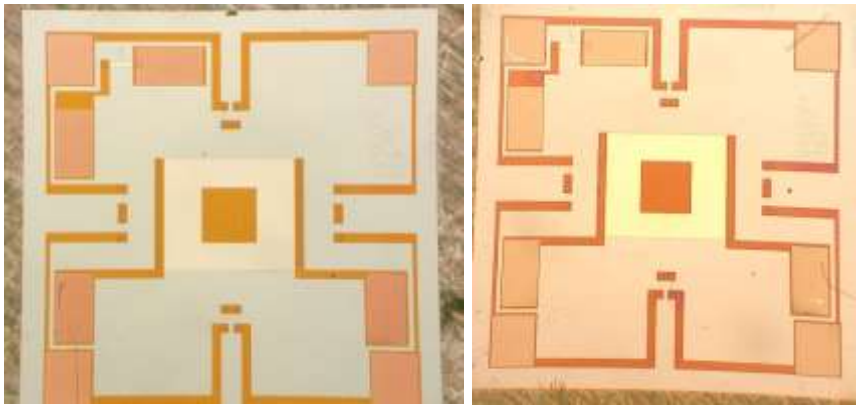

Figure 21 Fabricated Type 1(left) type 2(right)

A type 2 sensor produced in lot 3 from wafer P1 is shown in Figure 21.

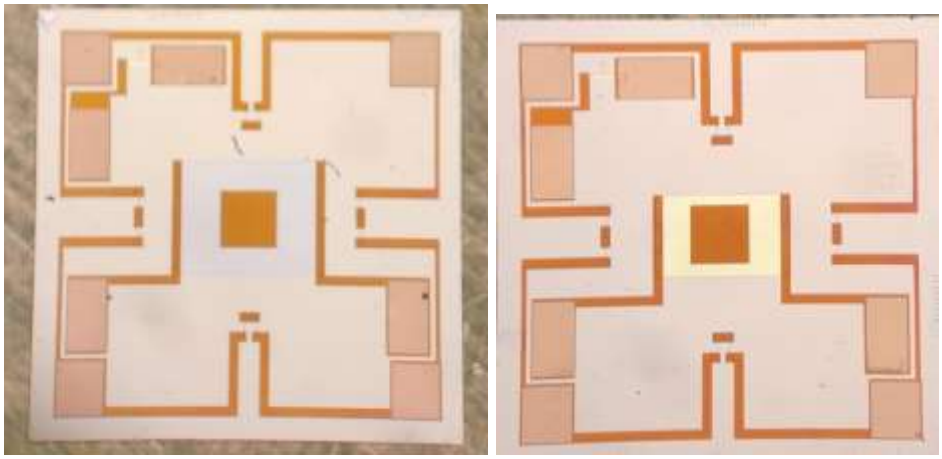

Figure 22 Fabricated Type 3(left) type 4(right) sensors.

Figure 22 shows a fabricated type 3 and type 4 sensor from lot 3 wafer P1. Figure 23 shows a fabricated type 5 sensor for lot 3 wafer P1.

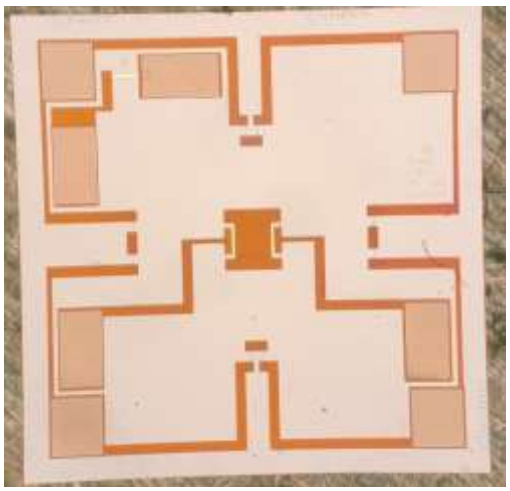

Figure 23 Fabricated Type 5 Sensor

Variations of lots

6.2 Diaphragm thickness

For Lot 1 it had a large variation of thickness across the wafer. It had diaphragms that where 10 µm-40 µm thick. Due to this variation, there was sensor to variances causing them to operate differently. The thickness of the diaphragms was measured by breaking a sensor in half and placing it under a microscope with measurement software. It was then measured at three

points across the diagram to get the average thickness as shown in Figure 24. The measurements taken across the wafer are shown Figure 25.

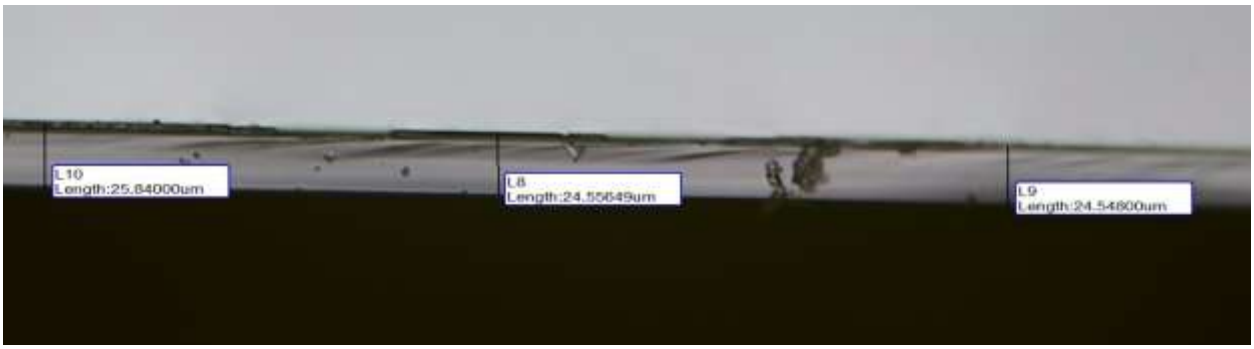

Figure 24 Diaphragm thickness measurement

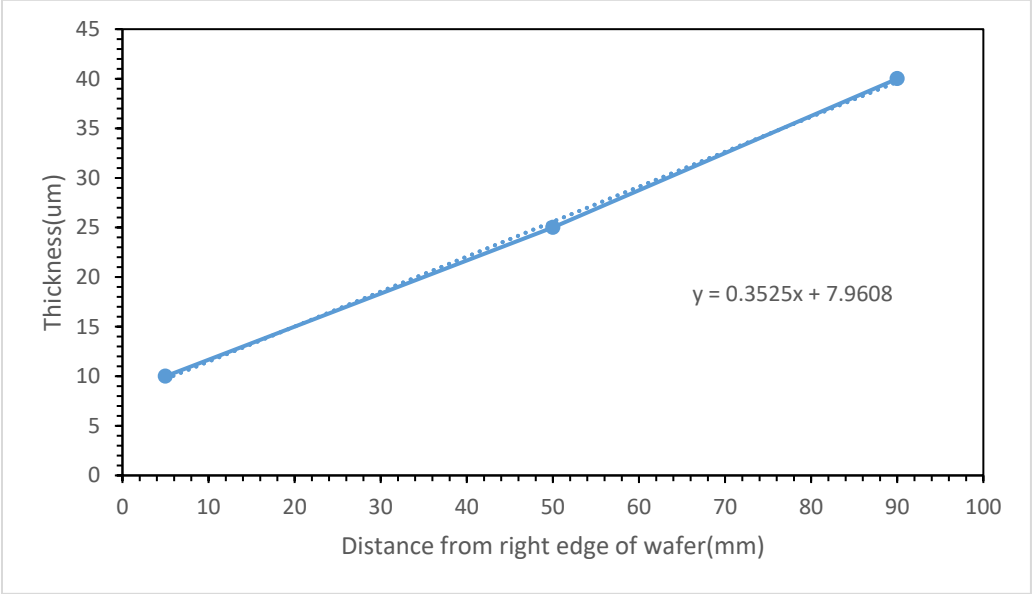

Figure 25 Thickness of Diaphragms across Lot 1 wafer 2

The diaphragms above 20µm were too thick and could not oscillate properly. The sensors that where too thick had the diaphragm thinned down using a plasma etch process to get then in the 10 µm to 15 µm range. This is due to the sensors resonating frequency being determined by the thickness and initial design was for 15µm diaphragms. Lot 2 also had variations of diaphragm thickness similar to lot 1. This would cause sensor to sensor variation making it difficult to compare sensors of the same type to each other. The sensors with a thinner diaphragm would operate at lower heater voltage compared to the thicker ones.

6.3 Lot 1 offset diaphragms

Due to the front and backside mask alignment being done by hand the diaphragm where not always centered. This caused a change in the method of vibration leading to some of parts of the Wheatstone bridge not experiencing the same amount of strain. I some cases one or more of the resistors would not experience any strain, this would cause the output of the bridge to be unbalanced and not reflect the true oscillations.

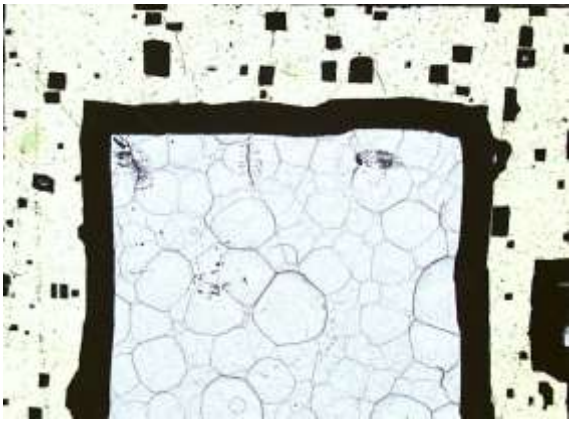

Figure 26 Lot 1 sensor with offset diaphragm

6.4 Variation of resistance across wafers

Lot 2 had resistance variations across the wafers. This was due to the ion implanter being down spin on dopant was used instead. The resistance variations are shown in Figure 27. At the top of the wafer opposite the flat it had an average resistance of 669 Ω for the bridge while closer to the center of the wafer it had a resistance of 1154 Ω for the bridge. The center of the wafer was not usable due to the bridge having an average resistance of 228 Ω. By the bottom of the wafer near the flat it had an average bridge resistance of 492 Ω.

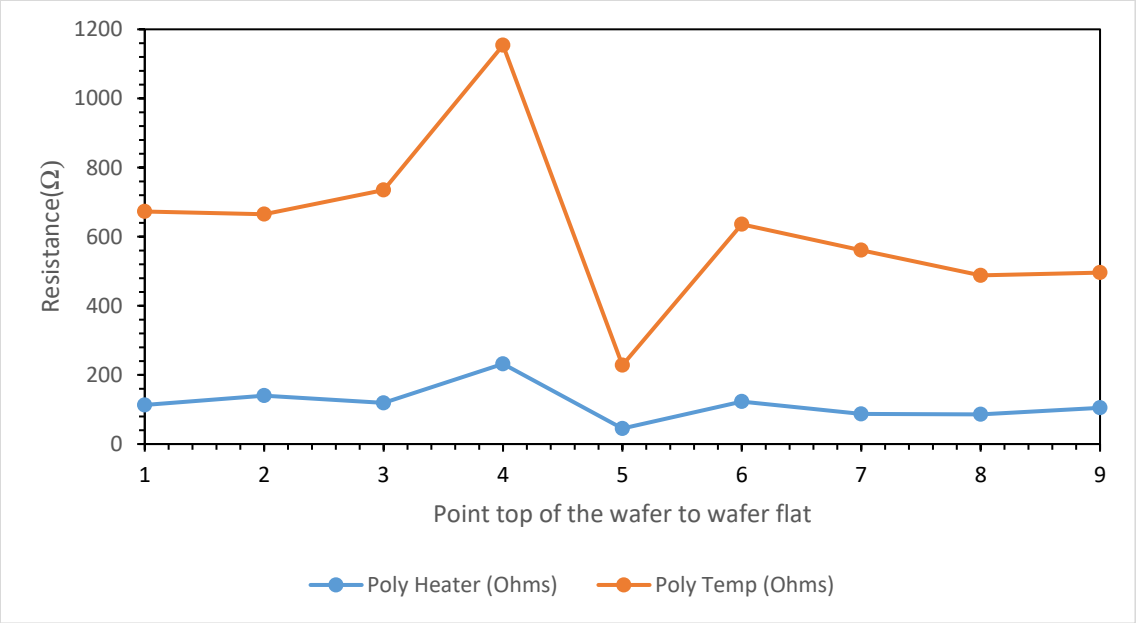

Figure 27 Resistance across Lot 2 wafer P1

Because of the large variation of resistance sensors from the same type would not operate the same. This causes any data collected from Lot 2 to be unreliable. Lot 3 fixed this issue by using ion implantation instead of spin on dopant. The more uniform resistance for lot 3 is shown in Figure 28.

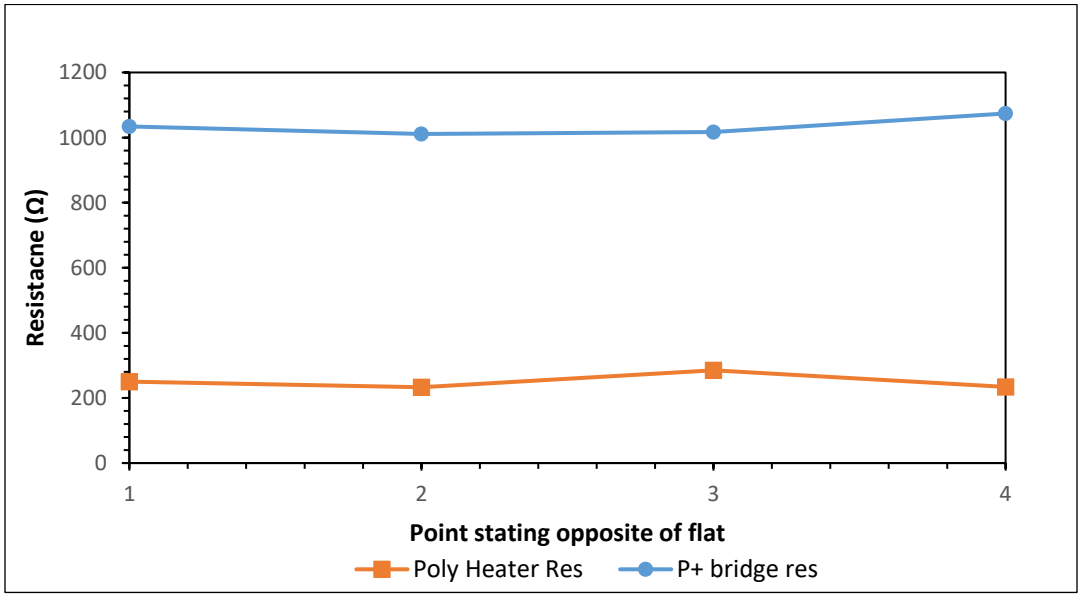

Figure 28 Poly resistance across Lot 3 wafer P1

6.5 Improvements of fabrication process

To improve the quality of the sensors produced a second lot of fabrication was done. Lot 2 had improvements over lot 1 sensors by having improved diaphragm alignment. This was accomplished by using the Suss MJB4 which has the ability to shine an IR light through the wafer that the alignment camera can see. This allows for better front to back alignment of the mask layers. This eliminated the offset diaphragms that were observed in lot 1.

To further improve diaphragm uniformity Silicon-on-Insulator (SOI) wafers where bought from WaferPro [11] to be used in production of lot 3. These wafers come with an oxide layer buried 20 µm deep that acts as an etch stop during the KOH diaphragm ecth. This is because the 40% KOH etch process etches silicon (100) orientation at 1.2µm/minute while the oxide layer is etched at .006µm/minute [12]. Because the oxide layer effectively won't be etched through, the diaphragm cavity will be etched however the silicon above the oxide making the diaphragm won't be etched at all. This ensured a consistent thickness of 20µm for all diaphragms across the wafer. This allows the sensors to perform more uniformly as diaphragm variations can be ruled out.

Bare die testing

After the sensors where fabricated and wafers where diced the sensors were tested on a manual probe station for electrical testing as shown in Figure 29. The test begins by doing a resistance test on the bridge, heater, and temperature sensor to ensure there is no open or shorts. Once the die passes the resistance test it moves on to the full electrical test.

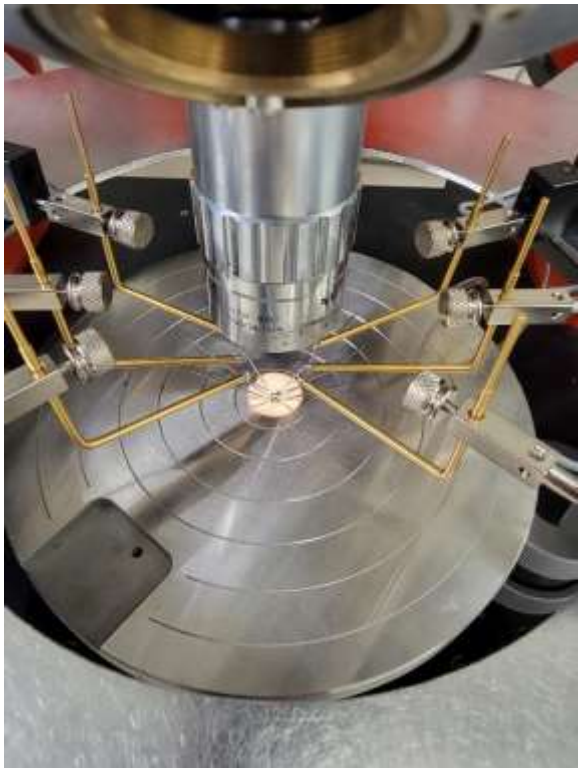

Figure 29 Manual Probe station

7.2 Testing results

From lot 3 the data collected from type 1 is shown Table 1

Type 1			
ID	**Bridge Resistance**	**Heater Resistance**	**Temp Resistance**
L3P1T1_1	1076	105	630
L3P1T1_2	1080	112	624
L3P1T1_3	1097	121	623
L3P1T1_4	1124	118	641
L3P1T1_5	1135	120	629
L3P1T1_6	1098	108	634
L3P1T1_7	1098	111	635
L3P1T1_8	1096	108	641
Average	**1100.5**	**112.875**	**632.125**

Table 1 Resistance measurements of Type 1 sensors from lot 3

The type one sensors had an average bridge resistance of 1100Ω. This process was repeated for each lot to ensure the devices were working properly.

Test Setup

8.1 Sensor Circuitry

The circuit of the sensor is shown in Figure 30. The sensors a plugged into to the test fixture show in Figure 31. The internal circuity of the fixture allows for powering and amplification of the sensor signal. Typically, 5 V is applied to the Wheatstone bridge to power the resistors and allow a more noticeable resistance change to be observed during oscillations. The V1 and V2 outputs of the Wheatstone bridge are sent to an operational amplifier. In this fixture an INA101HP is used as the op-amp. A 0-1 kΩ potentiometer is attached to the Op-amp to change the gain of the signal without have to change a physical resistor. The fixture is able to apply a gain up to 60 times. This allows for rapid and easy adjustment of the signal. To power the heater a IRLZ24PBF MOSFET is used along with a signal generator. The MOSFEF has a gate voltage of 5 V and has a maximum drain to source voltage of 60 V [13]. The signal generator will power the gate of the MOSFET allowing the heater to pulse on and off. It sends a pulse signal with a 5 V amplitude typically at 20 Hz for a pulse width of 20 µs. Along with the signal generator a 10 V power supply is attached to the MOSFET source to provide the power required for the heater. The output of the Op-amp is sent to an oscilloscope to read the signal. From the oscilloscope the data is sent to LabVIEW for data capture and analysis.

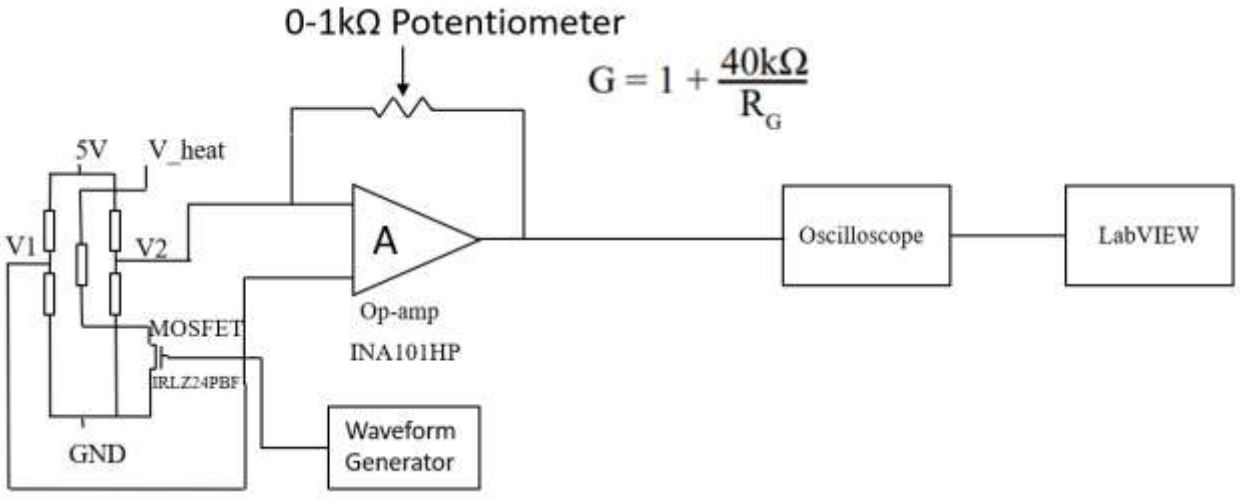

Figure 30 Sensor test circuit

8.2 Test fixture

To allow for ease of testing a test fixture was created to allow for faster and easier setup of each test. The test fixture is shown in Figure 31. This allows for the power supplies and signal generator to be easily connected to sensor circuitry. It includes a head pin connector to easily attach the sensors along with an external potentiometer to adjust the gain on the operational amplifier. Inside of the test fixture is the amplification circuitry along with the MOSFET used to turn the heater on and off based on the signal from the signal generator.

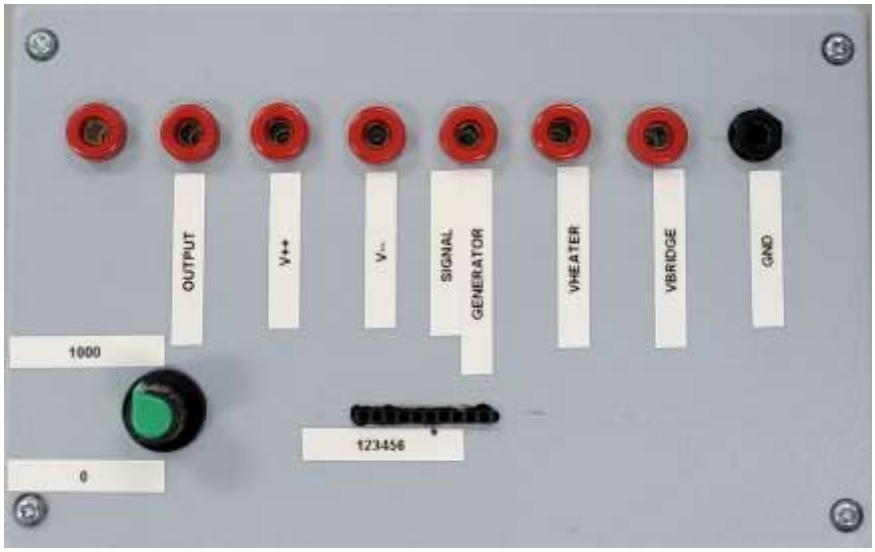

Figure 31 Electrical Test Fixture

8.3 LabVIEW integration

To facilitate quick data capture and control LabVIEW is used to read in the data from the oscilloscope. LabVIEW is able to capture the frequency, amplitude, and quality of the wave forms produced by the sensor. It also calculates the Fast Fourier Transform of the waveform. The UI for the program is shown in Figure 32.

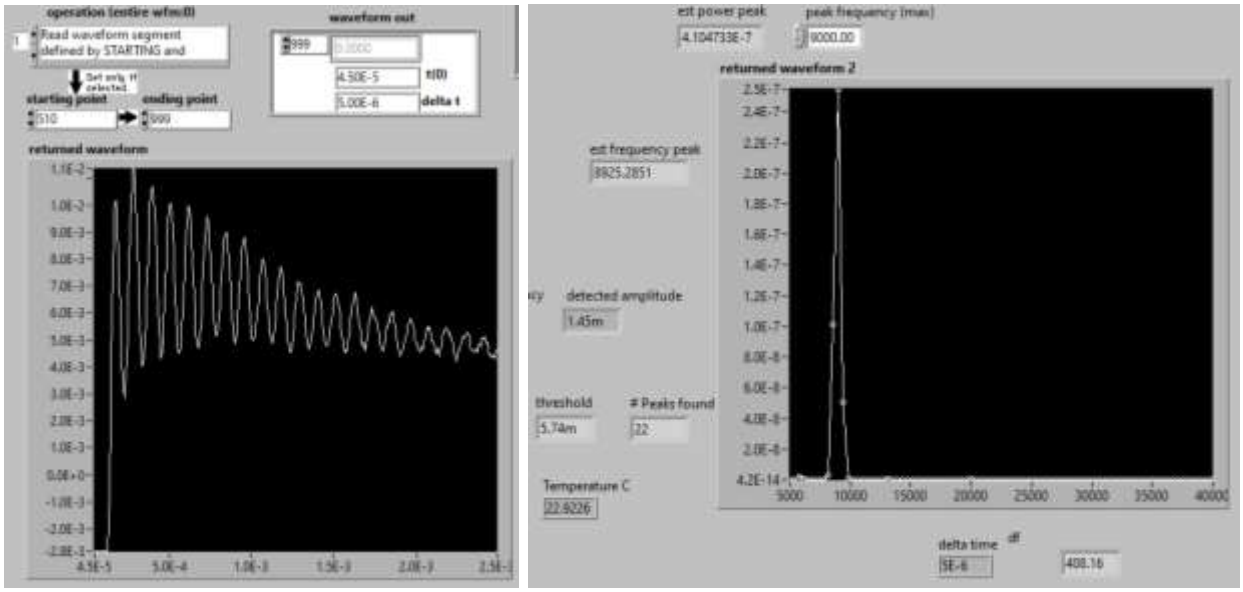

Figure 32 LabVIEW program

Sensor Packaging

9.1 PCB

When a sensor passes the bare die measurement it moves onto packaging to allow for further testing while also protecting the die. To package the sensor and allow for easier testing a PCB was designed. The PCB is a single layer It is a 14 mm x 76 mm single layer PCB with bare copper traces as shown in Figure 33. The board is made out of 1.2 mm FR4.

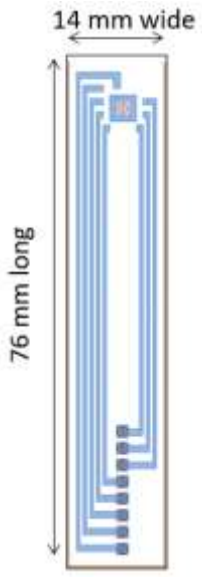

Figure 33 PCB

To assist with die alignment a copper rectangle was left as an outline of where to place the die. To allow fluid to flow in and out diaphragm a 1.6mm hole was added at the center point of the diaphragm mounting spot. Copper traces ran to the perimeter of the mounting location to facilitate easy wire bonding. This is shown in Figure 34.

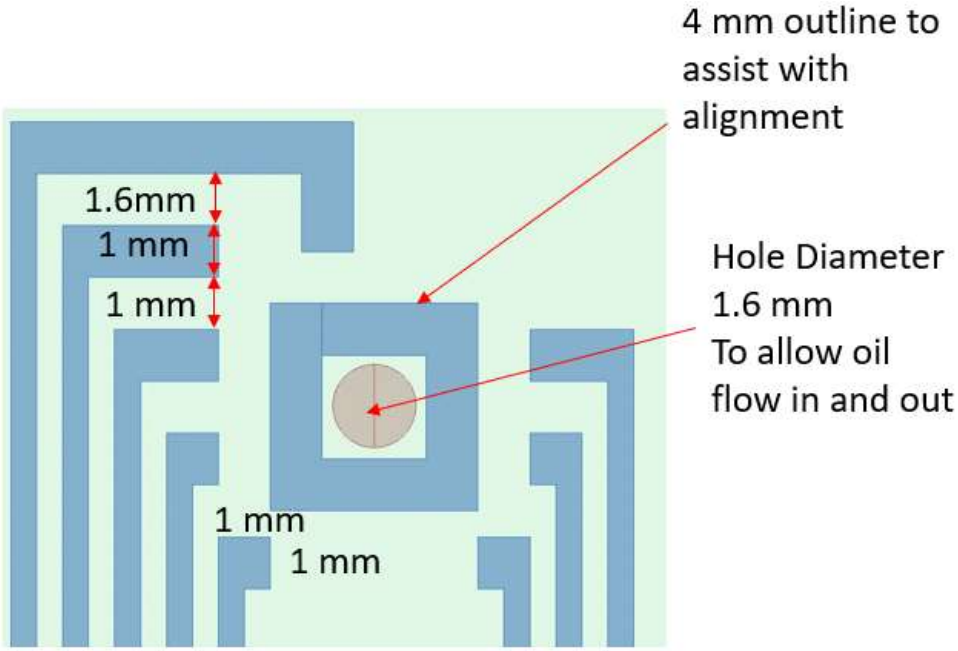

Figure 34 PCB layout

9.2 Packaging Process

To create a steady flow of packaged sensors a packaging process was developed to be done at RIT. The packaging process is done manually by hand and follows a few steps. First the die is attached to the PCB. To attach the die to the PCB a bead of epoxy is placed on the edge of die as shown in Figure 35. The epoxy must be carefully applied to prevent it from getting on the diaphragm.

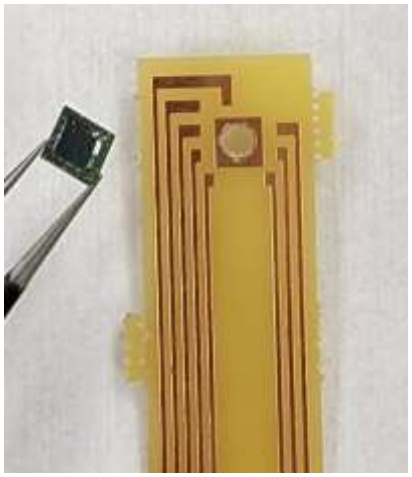

Figure 35 Die attach to PCB

The die is then placed on the PCB as shown in Figure 36. It must be placed over the centered over the hole to ensure the oil will couple with the diaphragm properly. It is then placed in the oven at 60°C for 5 minutes to cure the epoxy.

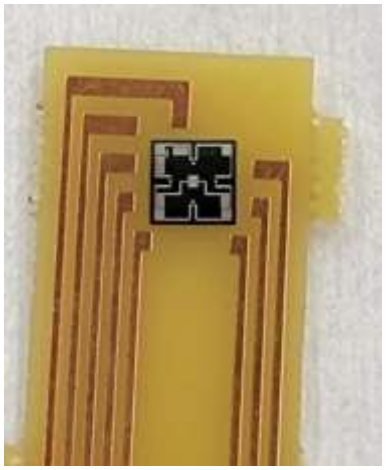

Figure 36 Die attached to PCB

After the epoxy has been cured the electrical connections are made through wire bonding. The completed connections are shown in Figure 37. To ensure the connections are working the sensor undergoes electrical testing. This is done by measuring the bridge, heater and temperature sensor resistance with a multimeter. By verifying the resistance of each it ensures there are no open or short circuits. Once the connections are verified it moves onto the next step.

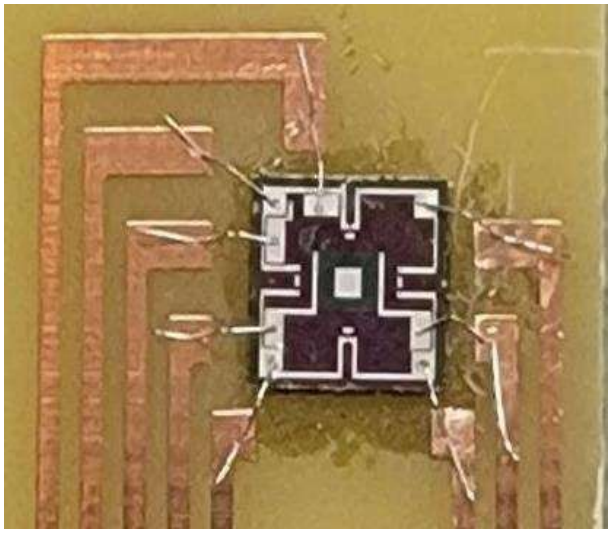

Figure 37 Wire boned Die.

To protect the wire bonds and prevent them from coming off the wires need to be encapsulated in epoxy. This is done by carefully covering the wires and connection pads with epoxy. The epoxy is kept away from the diaphragm to ensure it will still be able to oscillate as shown in Figure 38. With the Die encapsulated the wire bonds are now protected and oil testing can begin.

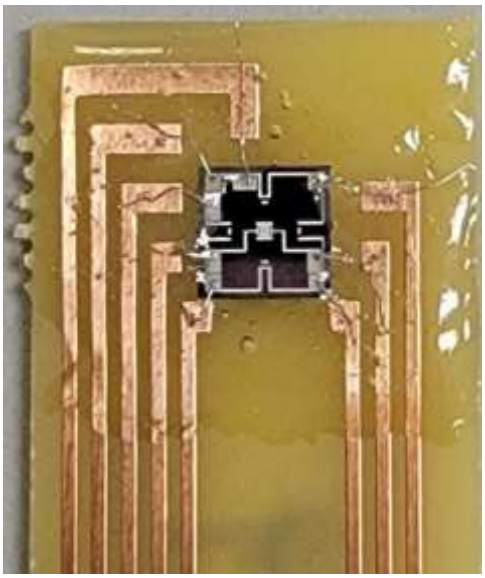

Figure 38 Encapsulated die

9.3 Packing effects on sensor operation

To determine if the packing process was creating any sensor-to-sensor variation a packaging study was performed. To track any potential changes 2 sensors from each type were tested at each step of the process. By using the same 10 sensors at each step, sensor to sensor variation will not affect the results. To also prevent the amount of signal amplification and heater voltages from affecting results, they were kept at the same values for each test. The study is started by collecting the data from the manual probe station testing. It is similar to electrical testing which includes attaching the sensor to the test fixture to allow the sensor to be run as if it were packaged to rule out any variation caused by test circuitry. Data is collated through the LabVIEW program capture its original frequency, amplitude and quality factor in air before the die attach step. This was done to determine if attaching the sensor to the PCB would affect its performance. Figure 39 show the response of 2 type 5 sensors in air before the die attach step.

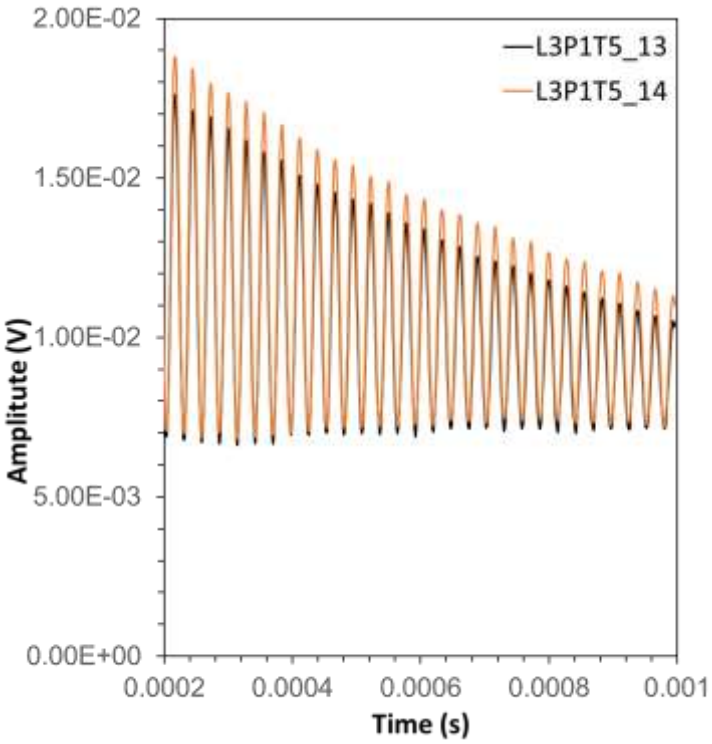

Figure 39 Bare die measurements of type 5 sensors

After the bare die measurements, the Die was attached to the PCB with epoxy. The data from the same type 5 sensors is shown in Figure 40

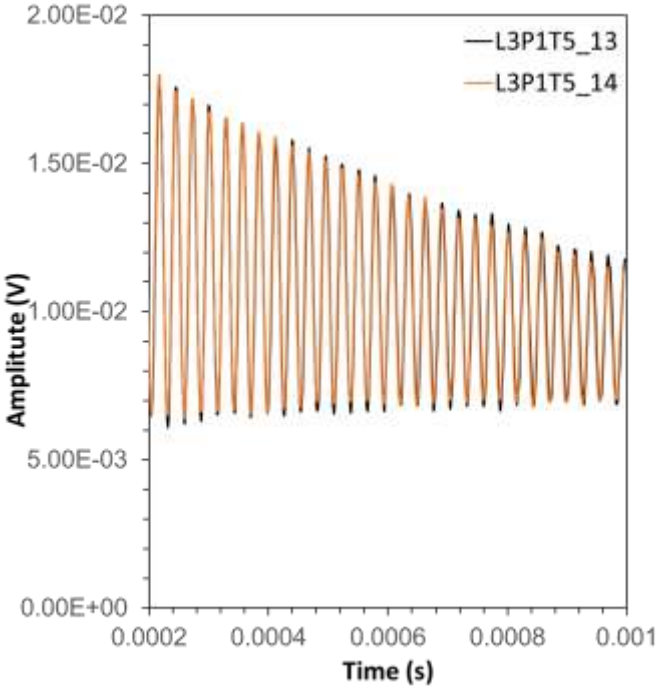

Figure 40 Type 5 sensors after Die attach.

From the data shown in Figure 39 and Figure 40 there is no noticeable change in response for either frequency, amplitude or quality factor.

The next part was wire bonding the die connections to the PCB to determine if they affect frequency, amplitude, or quality factor of the waveform. The die was wire bonded in house using an Orthodyne electronics M20B wire bonder. After wire bonding sensors were attached to the test fixture and run data collected for the type 5 sensors is shown Figure 41.

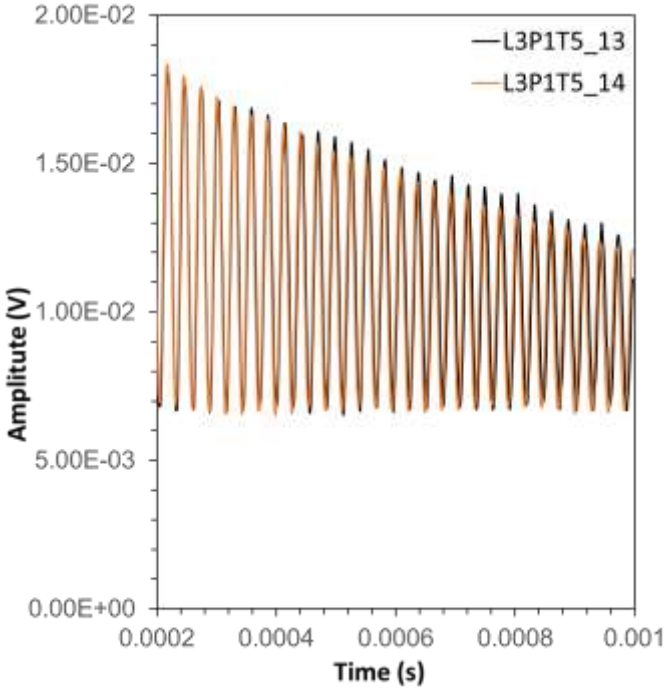

Figure 41 Type 5 sensors after wire bonding

From the data in Figure 40 there is no change in frequency, amplitude, or quality factor. This shows that the wire bonding process does not affect sensor performance.

After wire bonding the wires need to be encapsulated in epoxy to protect the connections. Because the epoxy will be covering the sides and part of the top side of the die it had the potential to affect the sensors performance. The data is shown in Figure 42 which shows no change in frequency or amplitude.

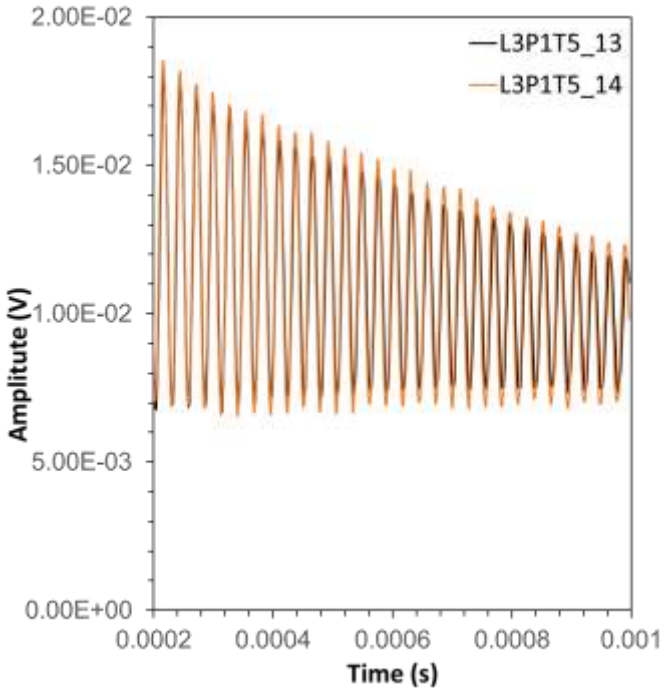

Figure 42 type 5 sensors after encapsulation

From the data collected there is no significate change in operation caused by the packing process. Any sensor-to-sensor variation is not caused by the packaging process.

Thermal analysis of fabricated sensors

10.1 Testing of integrated temperature sensor.

To evaluate the integrated temperature sensor voltage was run though it to track its change in resistance is it heated up. The purpose of the test was to determine what voltage to run sensor before it starts to self-heat. It's critical to run the sensor at voltages below self-heating ranges as it would affect the temperature being recorded. Its temperature was monitored using an IR camera and is shown in Table 2.

Voltage (v)	Current start (mA)	Current after 5 mins (mA)	Stable	Power (mW)
1	1.41	1.41	Yes	1.41
2	2.45	2.45	Yes	4.9
4	4.92	4.92	Yes	19.68
6	7.36	7.36	Yes	44.16
8	9.74	9.74	Yes	77.92
10	12.34	12.34	Yes	123.4
15	17.84	17.78	Heating	267.6
20	23.33	23.13	Heating	466.6

Table 2 resistor self-heating test

From the data collected the TCR for the temperature sensor was calculated using (2) which was 0.0473 %/K. The sensor was then placed in a lab oven and stepped through 6 different temperatures at increments of 10°C. This was done to collect enough data points to create a calibration curve of the sensor. The data was recorded and is shown in Figure 43.

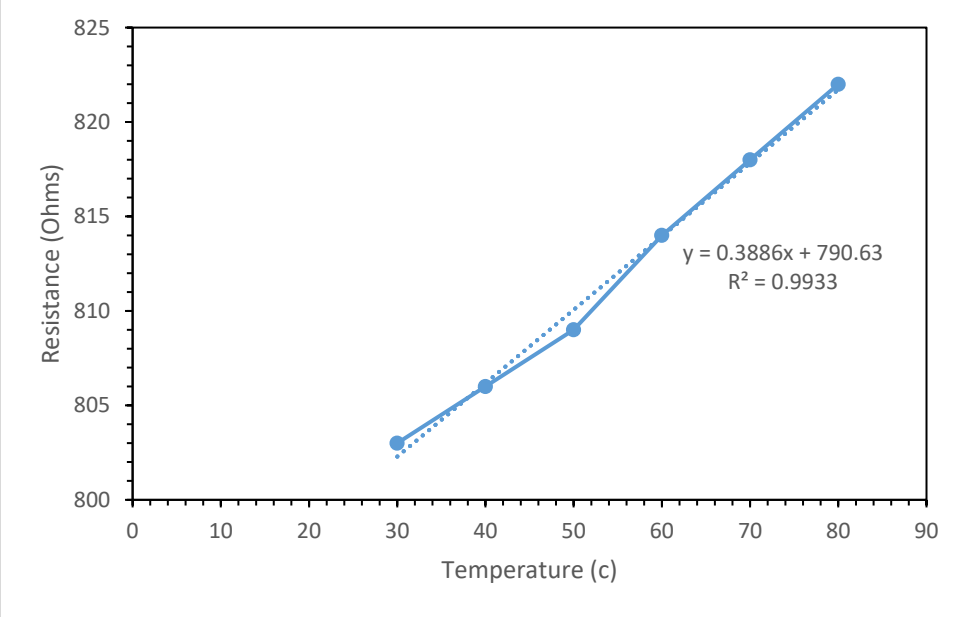

Figure 43 Resistance vs temperature for temperature sensor

Using the equation from the trend line in Figure 43 the temperature of the system can be monitored. This can be done by monitoring the change in resistance through the use of a voltage divider. The voltage divider would be balanced for room temperature and as the temperature of

the system increases the output of the voltage divider will increase. This is then correlated to temperature based on the calibration curve.

10.2 Thermal analysis of sensor diaphragm

The fabricated packaged sensors were placed under a FLIR camera to observe the heat dissipation of the sensor. The temperature of the heaters was compared to the calculated values in Figure 8. The setup used to measure the heaters is shown in Figure 44.

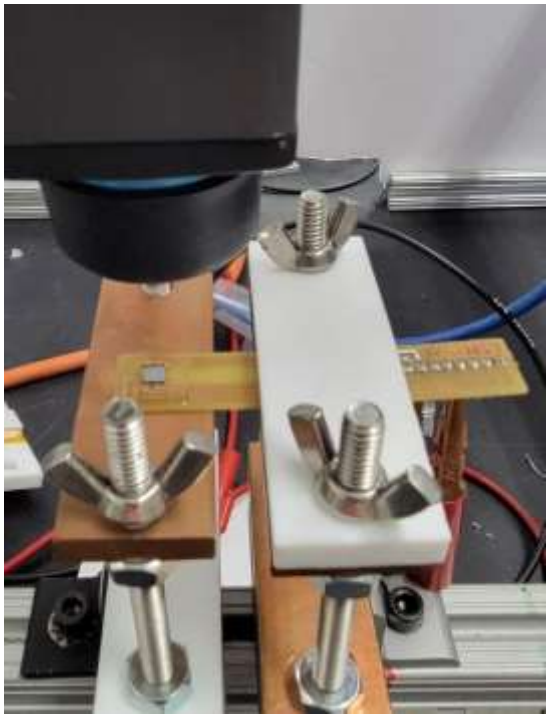

Figure 44 FLIR camera setup

The sensor is placed on a copper heatsink to simulate heat transfer as if the sensor was submerged in fluid. A power supply is attached to the heater and voltage is run through it. The temperature across the sensor is recorded.

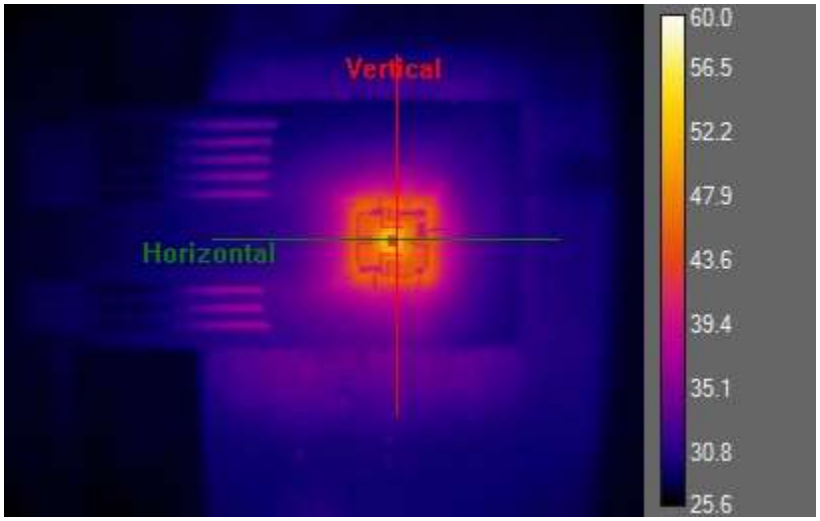

Figure 45 Type 1 at 5V

From the data and picture shown in Figure 45 the heat stays mostly confined to the center of diaphragm. However, it does rase the temperature of the epoxy that's encapsulates the wire bonds and the PCB is mounted on. At the center of the chip, it reaches a maximum of 52°C. It was also observed that the temperature sensor was at 47°C. Because of this the temperature sensor cannot be used to accurately measure the temperature of the system.

Sensor Characterization

To properly understand the performance of the sensors they were characterized by multiple methods to determine how each type performs. To keep track of each sensor a naming convention was made L# represents the lot of fabrication. P# or W# represent the wafer it came from T# is the type of sensor 1-5 and is followed by a dash number that represents the number of that sensor. L#P1T2_11 means lot 1, wafer P1 sensor type 2 and it the 11th type 2 sensor from this wafer that has been packaged.

11.2 Sensor operation in air

To evaluate each sensor type's base performance, they were run in air at room temperature. The amplitude of each sensor type is relative as it is influenced the amount of gain applied to the op-amp and the voltage run through the heater. To account for this both sensors form each type where run with the same gain and heater voltage.

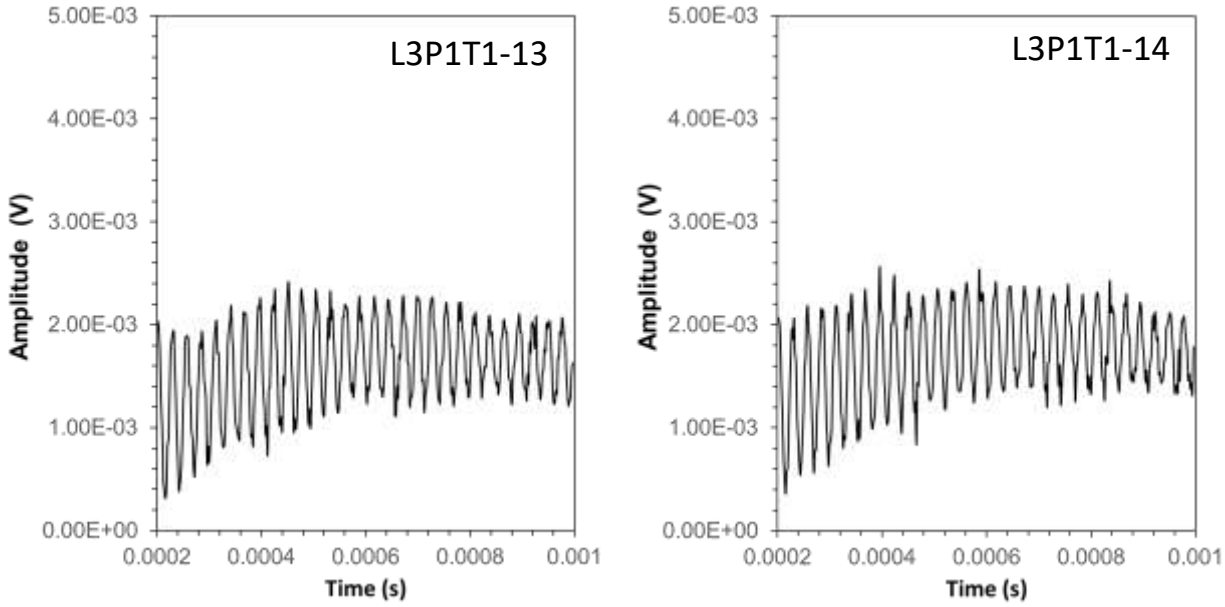

Figure 46 Type 1 sensors in air

2 type 1 sensors are shown in Figure 46. Both were run with the heater voltage at 20 V and the oscilloscope running an average of 16 to reduce any noise. They were both run at the same settings to prevent heater voltage and gain from affecting the amplitude of the signal. Type

1 has a generally lower signal due to using polysilicon resistors in the Wheatstone bridge which have a lower piezo resistive coefficient. Type one also has a smaller initial deflection due to using the larger 1.2x1.6 mm heater. The natural frequency both sensors operated at was 35 kHz.

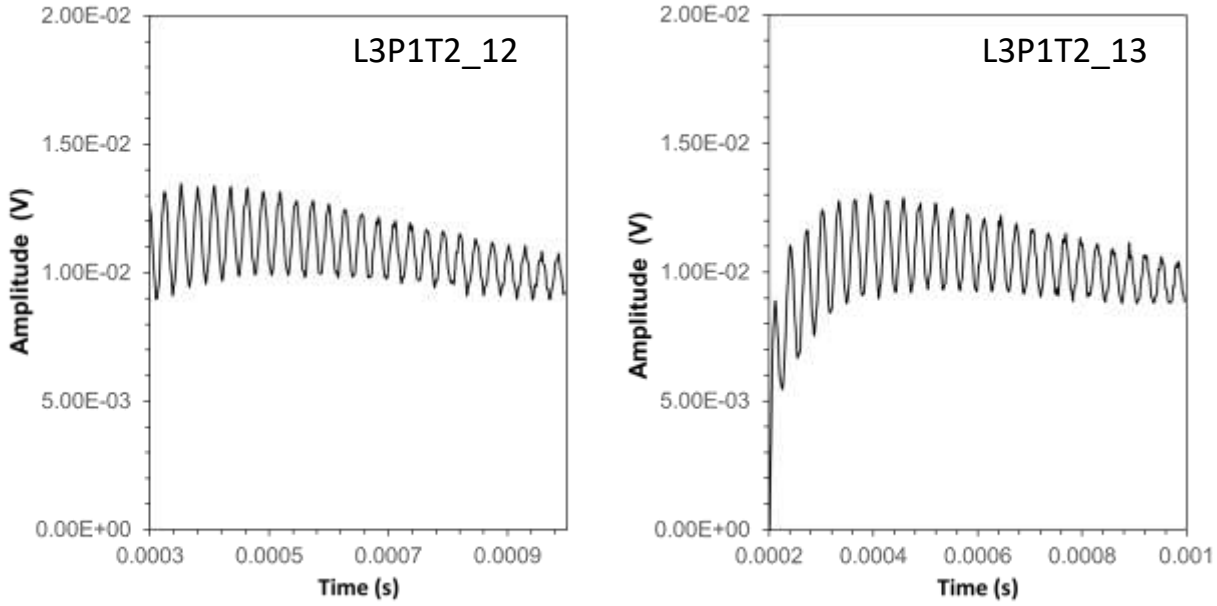

Figure 47 Type 2 sensors in air

2 type sensors in air are shown in Figure 47. Both sensors were run with a heater voltage of 18 V and average of 16 on the oscilloscope to reduce any noise. Type 2 uses the same 1.2x1.6 mm polysilicon heater as type 1 but it uses P+ resistors for the Wheatstone bridge. Due to having a more sensitive Wheatstone bridge the type 2 sensors can be run with a heater voltage 18 V, which is a lower voltage than type 1 and have a similar amplitude. Since type 2 runs at a lower voltage it can be useful for any applications where power consumption is a concern.

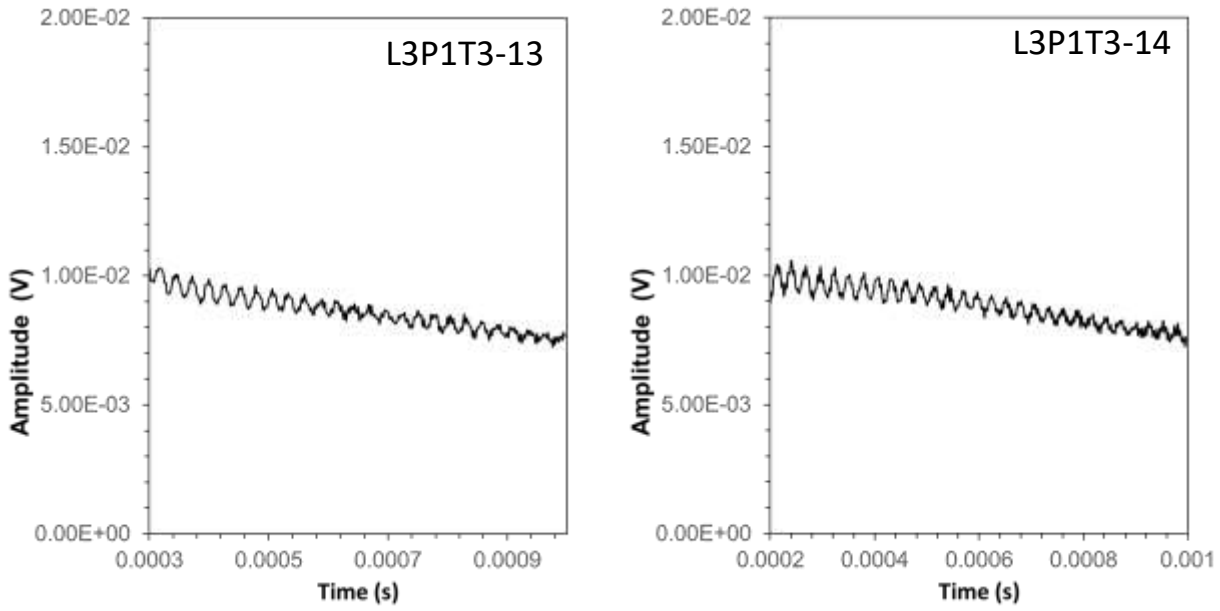

Figure 48 Type 3 in air

2 type 3 sensors are shown in Figure 48. They were both run with a heater voltage of 18V and average of 16 on the oscilloscope to reduce any noise. Type 3 uses the same P+ Wheatstone bridge as type 2 however it uses a different heater. It has a 1.2x1.6 mm P+ heater to test the effect of heater material. Due to the P+ heater creating a lower initial deflection. Type 3 has a low amplitude.

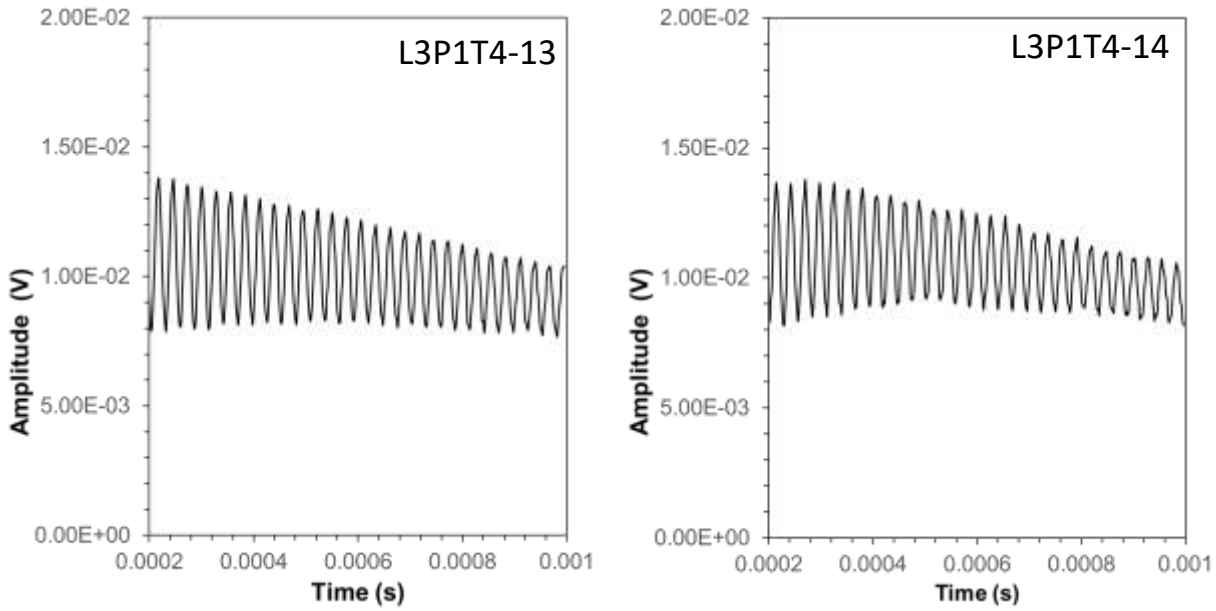

Figure 49 Type 4 in air

2 type 4 sensors in air are shown in Figure 49. Both sensors were run with a heater voltage of 15 V and average of 16 on the oscilloscope to reduce any noise. Type 4 uses the same P+ Wheatstone bridge as type 2 however it uses a smaller polysilicon heater. Type 4 uses a 0.8x1.3 mm polysilicon heater. Due to the smaller size of the heater, it produces a larger initial deflection than Type 2 allowing for a larger amplitude while running at a lower voltage.

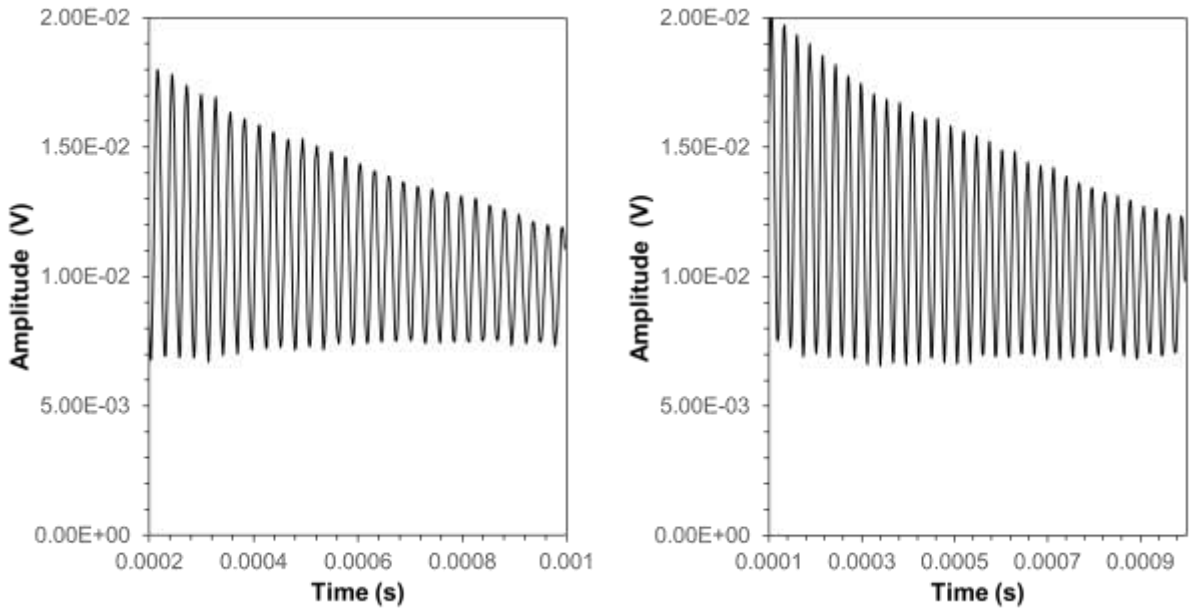

Figure 50 Type 5 in air

2 type 5 sensors in air are shown in Figure 50. Both sensors were run with a heater voltage of 10 V and average of 16 on the oscilloscope to reduce any noise. Type 5 uses the same P+ wheat stone bridge as types 2,3 and 4, however it uses the smallest polysilicon heater. It has a 0.29x0.5 mm polysilicon heater which produces the largest initial deflection. Due to the larger deflection type 5 can run at the lowest heater voltage and produce the largest amplitude.

11.3 Comparison of Wheatstone bridge material

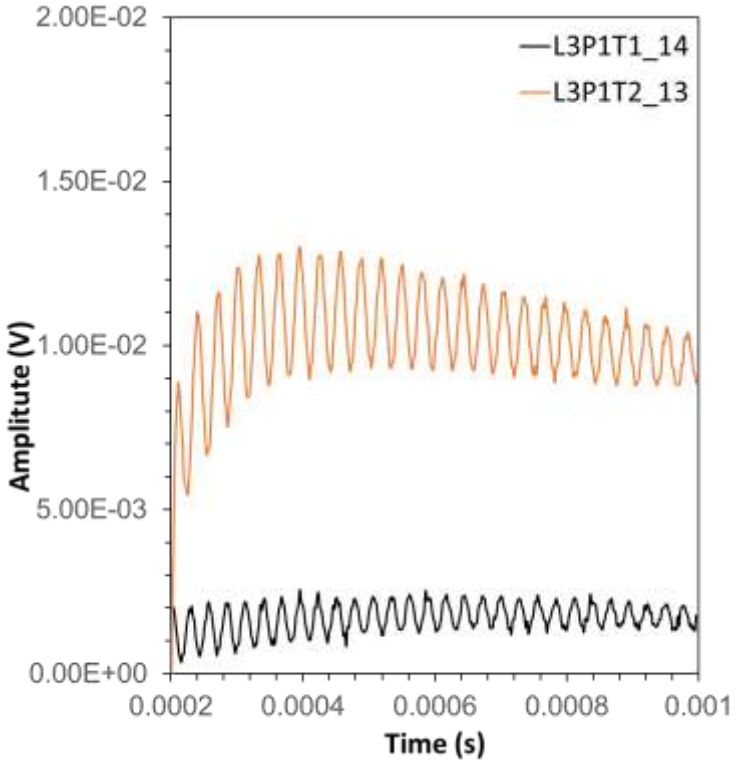

Figure 51 Comparison of Wheatstone bridge materials

To compare the effect of Wheatstone bridge material type 1 and type 2 sensors in air were plotted against each other and shown in Figure 51. For an accurate comparison both sensors use the same 1.2x1.6 mm polysilicon heater running at 20 V. The only variation between the types is the material used to create the Wheatstone bridge resistors. Type 1 uses polysilicon while type 2 uses P+ resistors. From the data shown in Figure 51 Type 2 has approximately double the amplitude as type 1. This can be attributed to the differences in the piezoresistive coefficient of both materials. P+ is a single crystal opposed to polysilicon which is made up of multiple smaller silicon crystals. Because of this P+ has a higher gauge factor resulting in a large change in resistance as the diaphragm oscillates.

11.4 Comparison of heater material in air

To evaluate the effects of heater material on sensor operation types 2 and 3 were run in air and plotted against each other. Both types use the same P+ resistors in the Wheatstone bridge and the same size heater. The only variation between the sensors is the material used to create the heater. Type 2 uses a 1.2x1.6 mm polysilicon heater while type 3 uses a 1.2x1.6 mm P+ heater. Both heaters where run at 18 V with the same gain, the data is shown in Figure 52. From the data polysilicon produces a larger initial deflection when compared to the P+ heater. Type 2 has approximately 3 times the amplitude. This shows that polysilicon produces a better heater when the application calls for a larger deflection of the diaphragm.

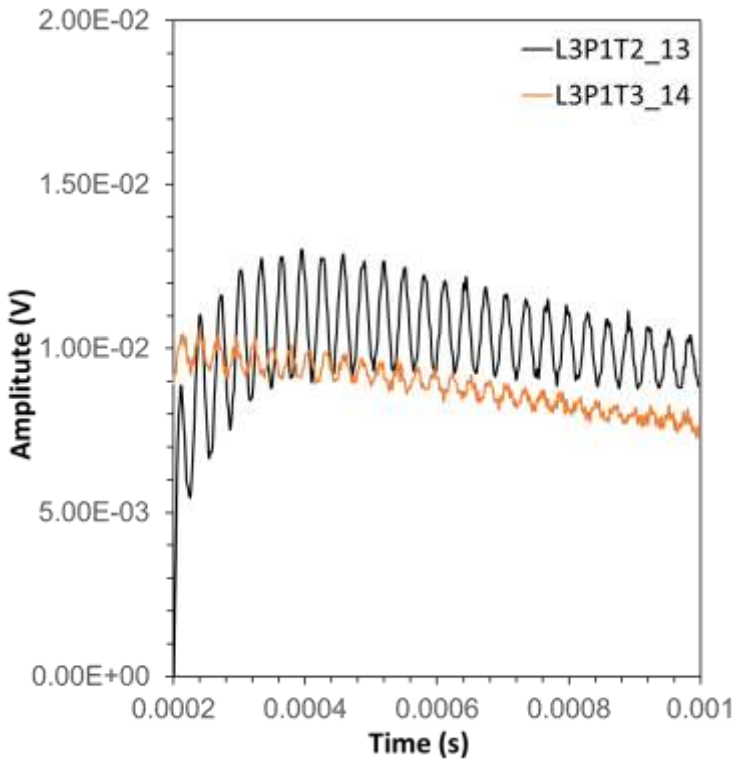

Figure 52 Comparison of heater material in air

11.5 Comparison of heater sizes in air

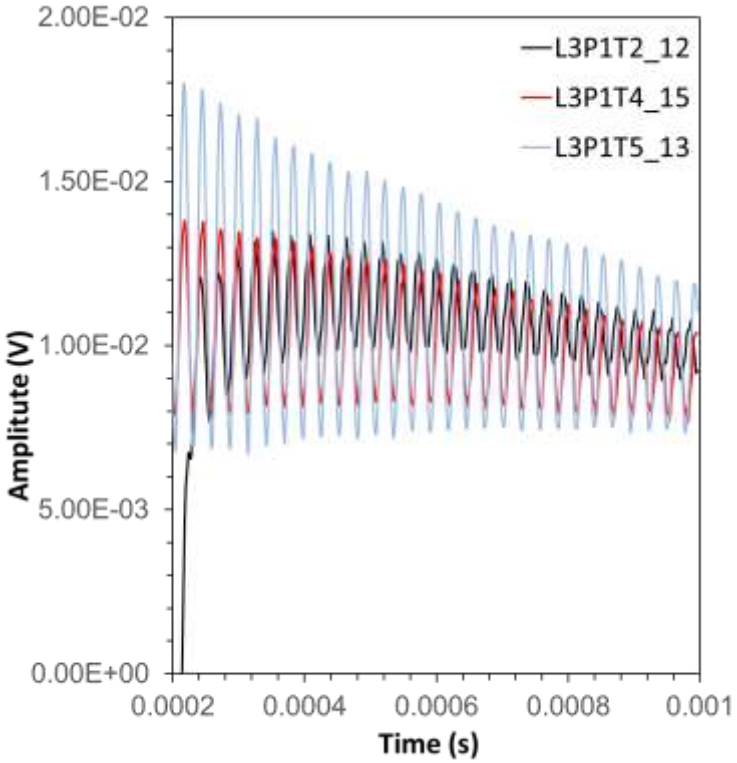

Figure 53 comparison of heater sizes in air

To compare the difference in heater size types 2, 4, and 5 are plotted against each other in air Figure 53. All 3 sensor types use the same P+ resistors for the Wheatstone bridge and the same material for the heater. The variation between the sensor types is the size of the heaters. Type 2 uses the largest polysilicon heater that is 1.2x1.6 mm. Type 4 uses a medium size polysilicon heater that is 0.8x1.3 mm. Type 5 uses the smallest polysilicon heater that is 0.29x0.5 mm. As the heater gets smaller the initial deflection of the diaphragm increases which is shown by type 2 having the smallest altitude while type 5 have the largest. This shows that as heater size decreases the amount of deflection increases as predicted.

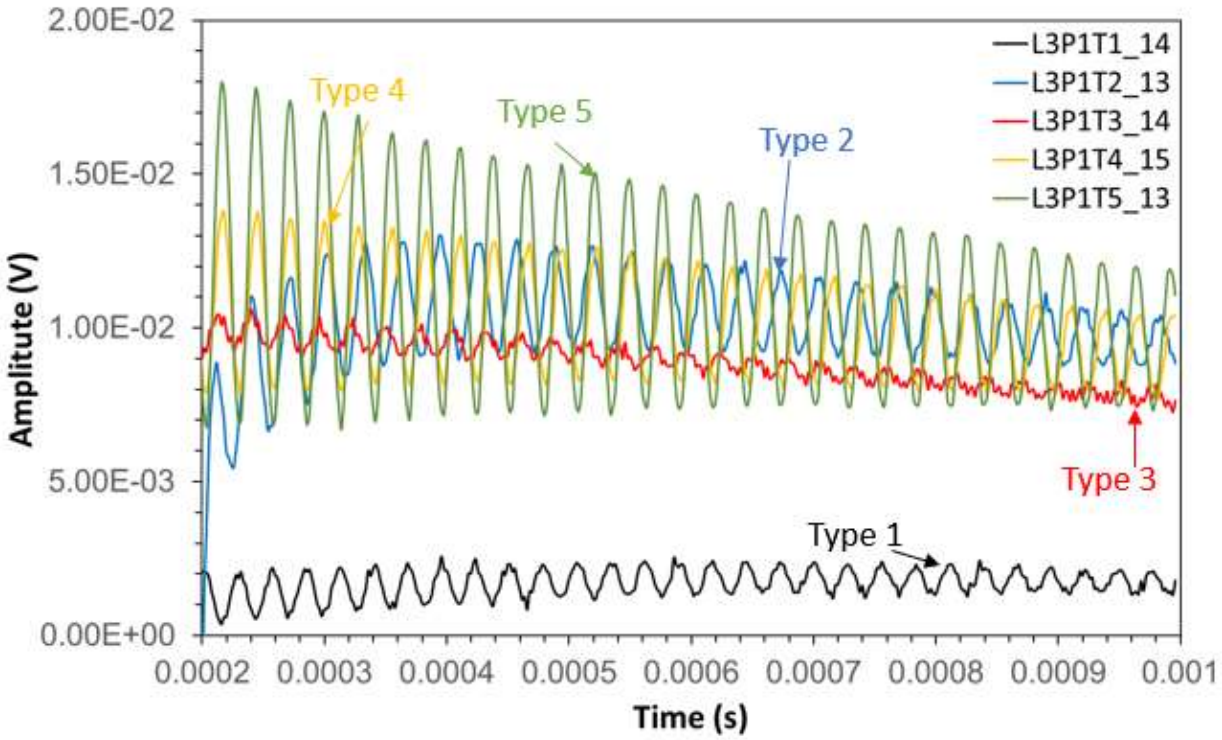

Figure 54 All sensor types in air

One sensor from each type in air were plotted against each other to easy comparison of operation as shown in Figure 54. For the largest signal amplitude types 4 and 5 should be used, however each sensor type still provides a large enough signal to accurately measure viscosity. To determine what type works best each one was run through multiple tests to determine how each operates in varying temperatures and viscosities.

11.6 Oil testing at room temperature

To get each sensor type's baseline response in oil each sensor type was placed into 8 different oils. This was done to determine the effective range of viscosities each sensor can detect. The testing starts with S6 that has a viscosity of 8.792 cSt which is the least viscous oil that was available for testing. The expected viscosity for each oil at 25°C is shown in Table 3.

Oil	Kinematic viscosity (25°C) cSt
S6	8.792
N10	17.01
N35	65.07
5W30	132.91
10W30	220
SAE40	400
N350	824.2

Table 3 Expected viscosity for oils at 25°C

Each sensor was placed in a jar containing the oil at room temperature and the sensor was left running the oil for 5 minutes to get the average response of the sensor. The waveform and FFT frequency from each sensor were captured to get the sensors baseline response. The FFT frequency of each sensor type vs the viscosity of the oil is shown in Figure 55.

Moving the senor between multiple types of oils had the potential of cross contamination which could affect the viscosity of each sample. If a higher viscosity oil got introduced into the thinner oil samples, it could increase the viscosity of the sample affecting the results collected. To minimize the potential of this happening the sensors were cleaned after each test in a few steps. First the oil left on the surface of the sensor and PCB was wiped away using an absorbent cloth. The cloth was also carefully placed into the diaphragm cavity through the hole in the PCB to absorb any oil trapped. Next the sensor was rinsed with deionized water to wash away any oil that was not absorbed by the cloth. The sensor was then dried using another cloth before being powered back on to prevent the water from shorting the sensor. Once it was confirmed that the sensor was cleaned it moved onto the next oil.

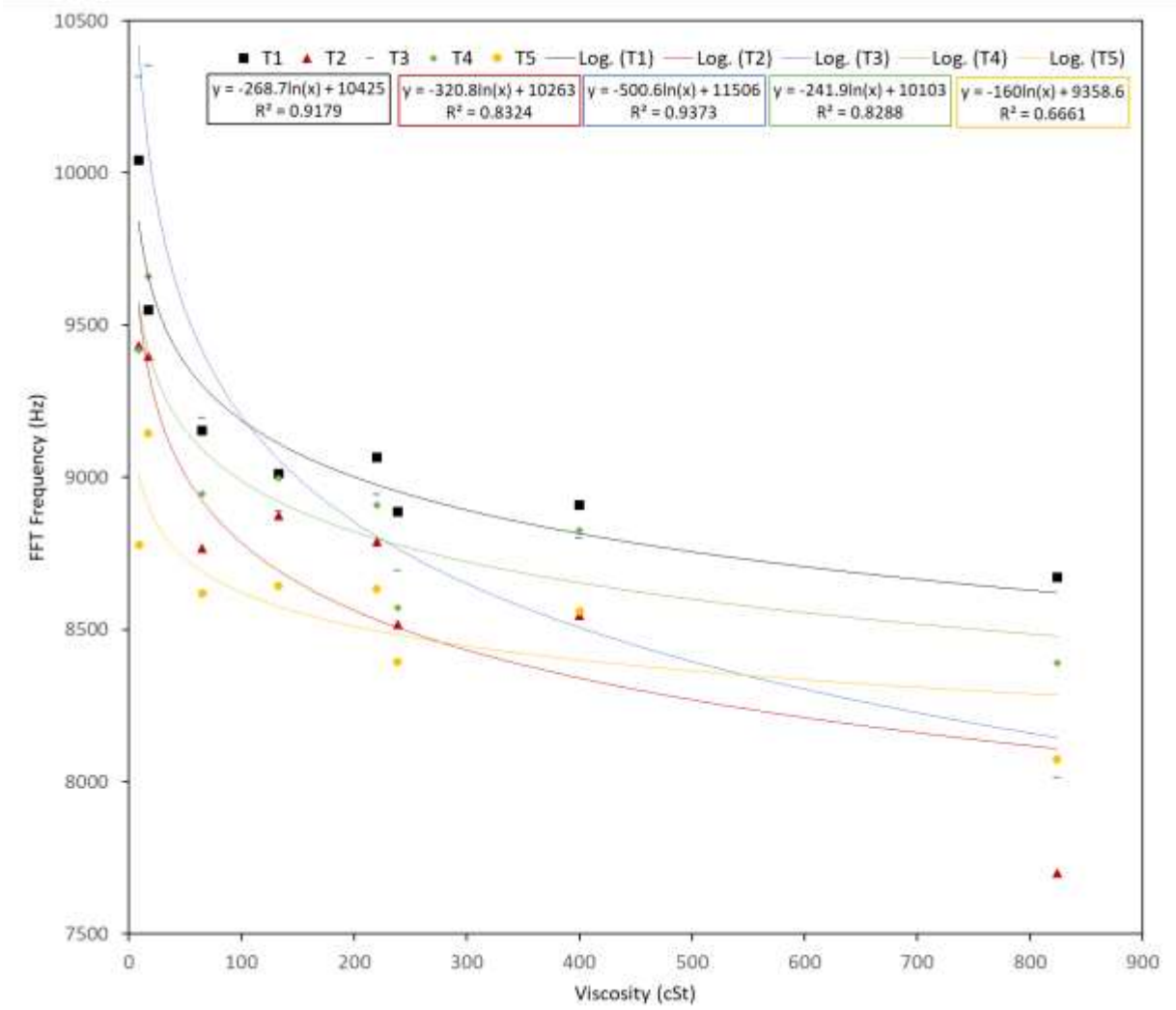

Figure 55 Baseline oil testing of each sensor at 25°C

One sensor from each type is shown in Figure 55. A logarithmic trend line was fitted to each sensor's data in order to model the response of the sensor for a given viscosity value. This testing did not prove to be the most accurate way of charting the base line repose of each sensor type. Type 5 could not be accurately modeled as it had an R^2 value of 0.66. This could also be due to the viscosity values of some of the oils at room temperature no longer being what they should. The S6, N10, N35 and N350 had been sitting in the lab for couple of years. Per the ASTM standard that they are made they have a limited shelve life before their viscosity changes. Due to this their values cannot be considered completed accurate and new samples were ordered for the standard oil temperature sweep experiment. Because of this variation this method was not used.

11.7 Oil mixtures

To determine the minimum viscosity change each type can detect an oil mixture experiment was created. The principle of the experiment was to start with a known quantity of oil to create a baseline. The sensor would run in the baseline for 30 minutes to chart its response and observe any fluctuations. Next a small amount of thicker oil was added, and the sensor would be monitored for another 30 minutes. This process would repeat until the mixture became 90% of the staring oil and 10% of the added oil. This test was run with a lot 3 type 5 starting with 50mL of 5W30 oil as the baseline. 0.25mL of 10W30 oil was added every 30 minutes until 12:30. Then the 1 mL was added every 30 minutes for another 2 hours. The data collated is shown in Figure 56. From the data the FFT frequency gradually decreased. The temperature of the oil was also monitored to account for any minor fluctuations in viscosity. Minor fluctuation is temperature where cause by the temperature of the room changing through the day.

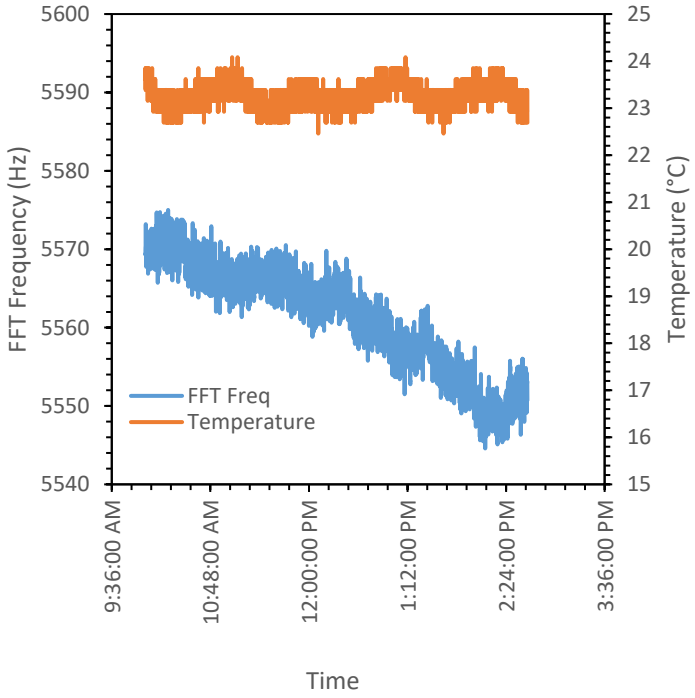

Figure 56 Oil mixture test with Type 5 sensor

After testing the oil mixtures in a lab grade rational viscometer, it was discovered that that the viscosity trends of each mixture do not follow the predicted trend. It was expected that when the thicker 10W30 oil is added to the 5W30 base line oil the viscosity of the mixture would

increase. However, testing revealed that the viscosity of the mixture would decrease as shown in Table 4.

Sample	Trial	Dial reading (%Torque)	Viscosity (cP)
Base 5W30	1	73.5	110.3
	2	73.7	110.6
	3	73.6	110.4
Base 10W30	1	83.2	124.8
	2	82.6	123.9
	3	82.4	123.6
25 mL 5W30 +1.25 mL 10W30	1	68.5	102.8
	2	69.5	104.3
	2	70.5	105.8
25 mL 5W30 +3 mL 10W30	1	68.3	102.5
	2	69.6	104.3
	3	69.6	105.8
25 mL 5W30 +5 mL 10W30	1	70.1	105.2
	2	71.6	107.4
	3	72	108

Table 4 Viscosity of oil mixtures

The suspected cause of this trend might be due to the different additives the manufacturer put in the oils. These additives are normally there to help increase the protection and life of the oil however it could be causing the oils to separate, lowering the viscosity. Because of this trend, this method is not a reliable way of testing for the minimum viscosity change each sensor can detect.

11.8 Temperature sweeps in Air

To subtract the effect of temperature on the sensors they were run through temperatures sweeps in lab oven to chart each sensor's response to changing temperatures. This response will be subtracted from viscosity measurements to remove the effects of temperature on the sensor. The test was conducted by placing the sensor in the lab oven. The test setup is shown in Figure 57. The sensor was placed on a metal heatsink to help dissipate the heat from as sensor as if it

was submersed in oil. A temperature diode connected to a DAQ was used to record the temperature with the LabVIEW program.

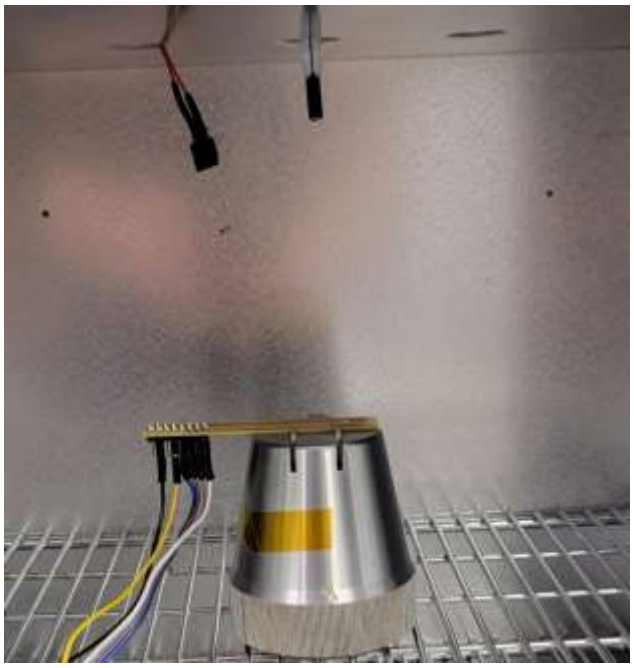

Figure 57 Oven temperature sweep test setup

The temperature started at 23C and was ramped up to 80C. The oven would remain at 80 for 5 minutes to ensure that the system has stabilized before continuing. Once the system stabilized the heat was turned off and the sensor remained in the oven until it cooled down back to room temperature. This ensured controlled heating and cooling of the sensor to eliminate any possible variance. Data is shown from the following temperature sweeps due to these sensors also being used in the standard oil temperature sweeps. From additional testing most sensors of the same type would operate similarly.

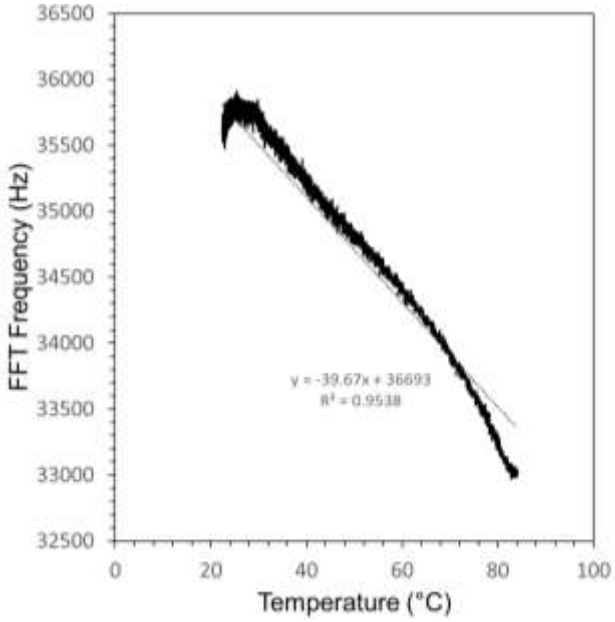

Figure 58 L3P1T1-22 in air

The FFT frequency from a type 1 sensor is shown in Figure 58. The sensor was run with a voltage of 18V. At room temperature it had an average FFT frequency of 3570Hz, while at 80°C it had an average FFT frequency of 3280Hz. A linear trend line was fit, and it had a mostly linear change in frequency as temperature increased.

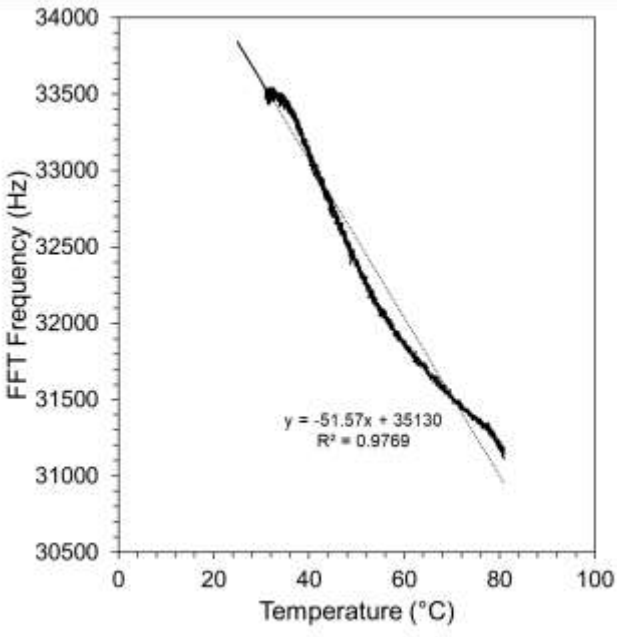

Figure 59 L3P1T2-11 in Air

Data from a type 2 sensor is shown in Figure 59. The sensor was run with a heater voltage of 18V. While at room temperature it had an FFT frequency of 33840Hz and while at 80°C it had dropped to 31197Hz. It had an overall change of 2643Hz which is a change of 7.81%. Using this data, the FFT frequency of the sensor at up to 80°C can be adjusted to account for this change.

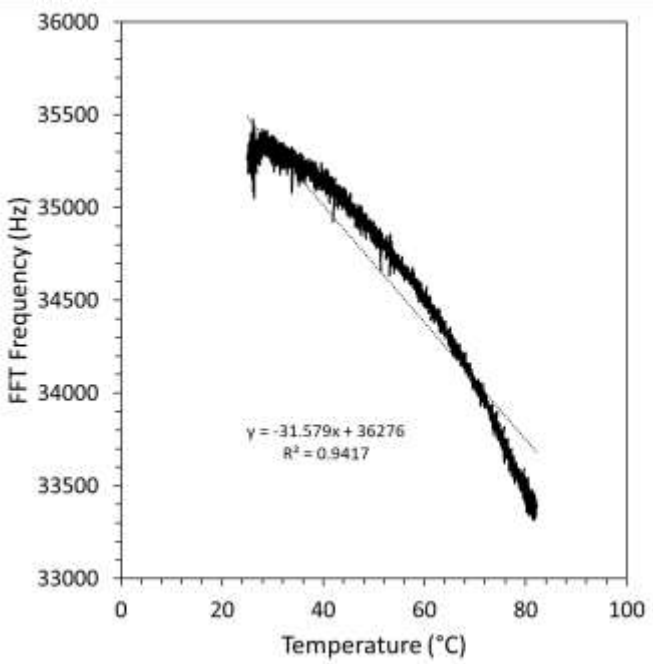

Figure 60 L3P1T3-11 in air

Data from a type 3 sensor is shown in Figure 60. The sensor was run with a heater voltage of 18V. at room temperature it had an FFT frequency of 35475Hz while at 80°C it had an FFT frequency of 33475Hz. From room temperature to 80°C it had a change of 2000Hz

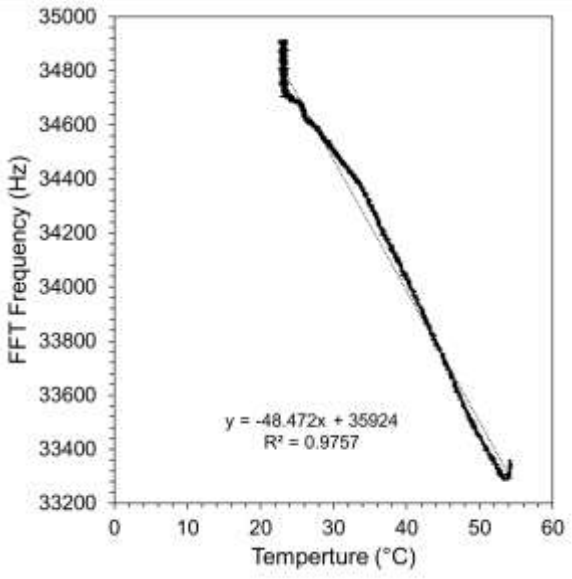

Figure 61 L3P1T4-20 in air

Data from a lot 3 type 4 sensor is shown in Figure 61. This sensor was run with a heater voltage of 15V. During testing it was discovered that the sensor could only operate reliably up to 55°C. Once the sensor went past 55°C the waveform would completely disappear. This could be caused by either the way the heater is interacting with the diaphragm at higher temperatures, or it could be caused a defect in this sensor.

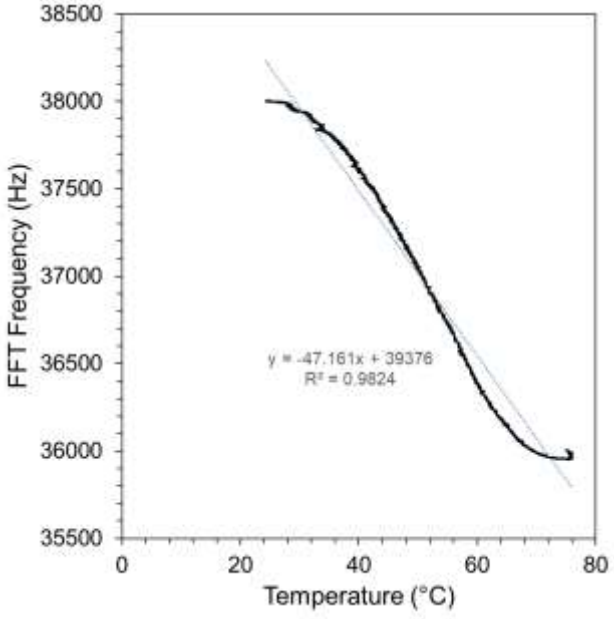

Figure 62 L3P1T5-21 in air

Data from a lot 3 type 5 sensor in air is shown in Figure 62. This sensor was run with 15V through the heater. At room temperature it had an FFT frequency of 38004Hz while at 80°C it had an FFT frequency of 36025Hz. From 25-80°C it had a change of 1979Hz. However, it is observed that once the sensor reached 70°C the FFT frequency started to level off and remain around 36000Hz. Because of this the sensor can only reliably work up to 70°C as the temperature correction will not be able to correct for a temperature variation reliably.

11.9 Temperature correction

Using the data collated from the temperature sweeps in air, a calibration curve can be crated for each sensor to account for the change in frequency due to temperature. The correction was done by first normalizing the change in change in frequency with the change in temperature. Then for each set temperature the % change in frequency was determined. This change was then added to measured frequency to account for the change in temperature.

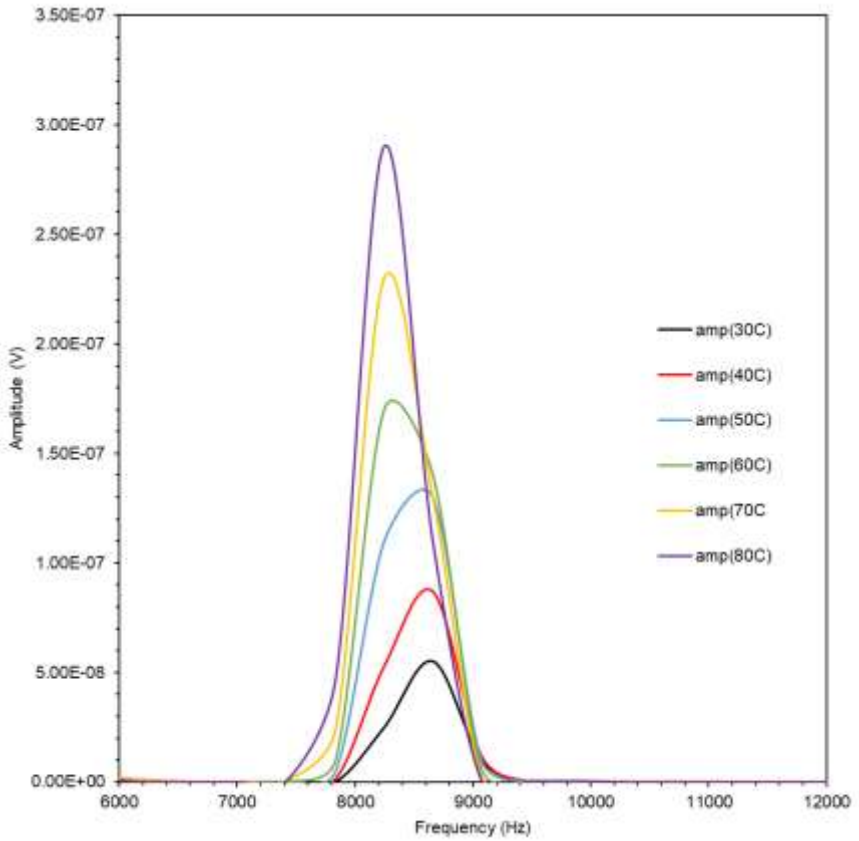

Figure 63 Type 1 sensor in N100 without temperature correction

Data from a type 1 sensor in N100 oil show in Figure 63. Without the temperature correction the frequency changes only a couple hundred hertz. This makes it difficult to detect any changes in viscosity as a change of 62.07 cSt from 30-40°C results in a change of 20Hz.

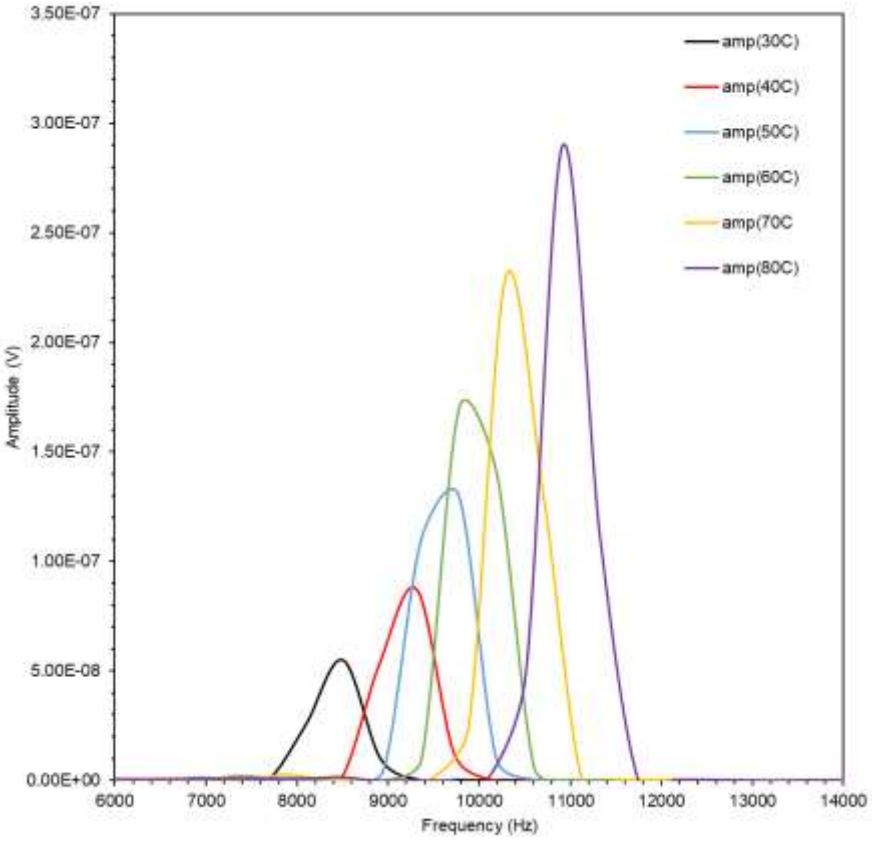

Figure 64 Type 1 sensor with temperature correction

The correction factor applied to the FFT frequency is shown in Figure 64. This effectively shifts the FFT frequency so that they increase with decreasing viscosity as expected. This allows changes in viscosity to also be more noticeable. Now the change of 62.07 cSt from 30-40°C is now 360Hz.

11.10 Detecting viscosity changes with standard oils

To better measure the smallest change each sensor type can detect. Viscosity standard oils were used. These oils are specially made and verified to track each oil's changes in viscosity at specific temperatures according to ASTM standards. By monitoring the sensors change at each

temperature its output can be directly correlated to a kinematic viscosity that has been verified. For testing N10, N35 and N100 oil was used. The three types were chosen based on how much their viscosity changes from room temperature. N100 had the largest change in viscosity across the temperatures while N10 had the smallest, with N35 being in the middle. By monitoring the different degrees of change the resolution of each sensor can be determined. The expected viscosity of each oil versus temperature is shown in Table 5. The values were provided by Cannon Instruments who created the oil samples used in testing. This method also eliminated the potential of cross contamination of samples since it would remain in one oil sample for the full temperature sweep.

Oil	Kinematic Viscosity (cSt)							
Temperature	20	25	37.78	40	50	80	98.89	100
N10	21.94	17.66	10.85	10.05	7.384	3.6	2.567	2.525
N35	86.5	65.66	35.47	32.19	21.64	8.619	5.603	5.477
N100	320.5	230.2	108.8	96.73	59.64	19.24	11.39	11.06

Table 5 Viscosity of N10, N35, N100 based on temperature.

Using the data from Table 5 the viscosity of each oil vs temperature was plotted with a power trend line to estimate the viscosity of the oil for any temperature between 20°C and 100°C. This was done because the oil temperature sweeps were done at intervals of 10°C starting at room temperature.

Testing began with N100 oil as it has the largest change in viscosity from 20°C to 100°C of 309.44 cSt. This has a linear change of 3.868 cSt/°C. Because of this N100 was used to see how each sensor type reacts to large changes in viscosity. The data from Table 5 was plotted with a power trend line fitted to allow for an accurate approximation of viscosity at 30°C,40°C,50°C,60°C,70°C,80°C. The trend line had an R^2 value 0f 0.9864 (Figure 65) showing that viscosity can be predicted accurately.

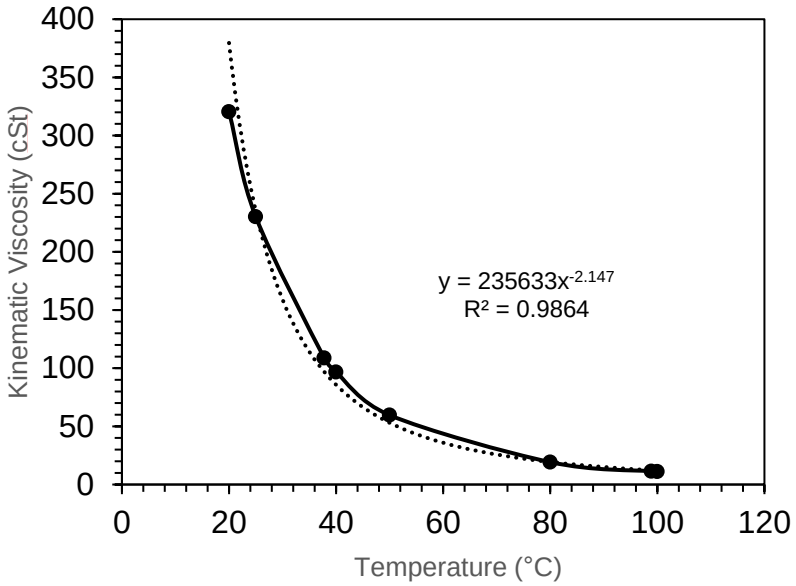

Figure 65 Viscosity of N100 dependent on temperature

One sensor from each type was placed into a jar containing N100 oil and placed into a lab oven at room temperature. The signal from the sensor was monitored using the LabVIEW program to extract the waveform and FFT at each temperature interval. A separate temperature sensor was placed into the oil to monitor its temperature as was captured with the LabVIEW data. The temperature of the oven was slowly increased to each temperature interval to allow the oil and sensor to heat up at a controlled rate. Once the oil reached the target temperature it remained there for 5 minutes to ensure it had stabilized before collecting data. Once it was conformed that the temperature has stabilized the waveform and FFT were extracted.

Using the curve from Figure 65 the viscosity for each temperature was estimated. Using the viscosity value for that temperature the FFT frequency collected at that temperature was than correlated to the viscosity value. The extracted FFT frequency vs viscosity of each sensor type in the N100 oil is shown in Figure 66. A power trend line was fitted to each curve and their R^2 values displayed to determine which sensor type was more sensitive to viscosity changes. From the data Type 2 is the most accurate fit due to having an R^2 value of 0.99. Type 5 was the second most accurate with an R^2 value of 0.98 followed by type 1 with R^2 value of 0.97, then Type 4 R^2 value 0.96. Type 3 was the least accurate with R^2 value of 0.90.

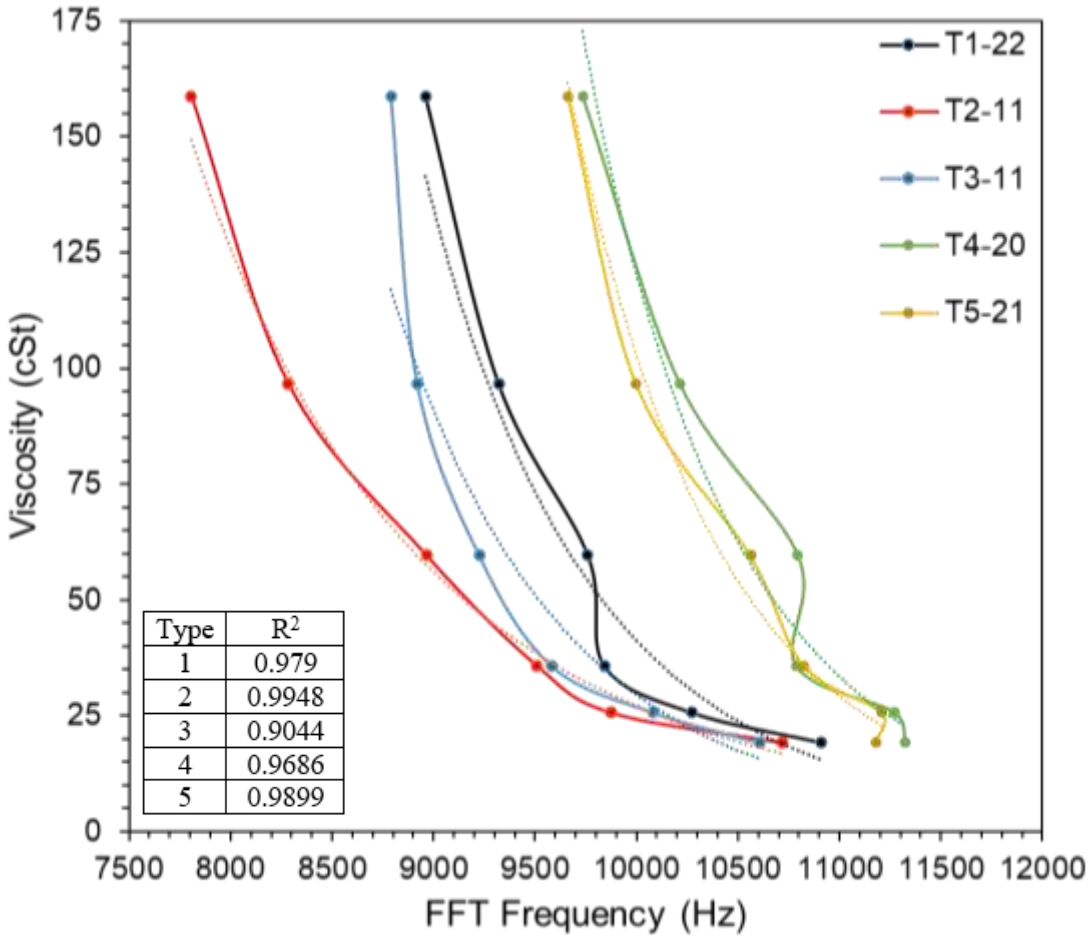

Figure 66 all sensor types in N100 oil temperature sweep

From Figure 66, it is observed that for types 4 and 5 that the frequency for 27.5 cSt and 19.24 do not follow the expected trend. This could be due to these measurements being taken at 70°C and 80°C respectively Which was required to get the N100 to reach desired viscosity. From the temperature sweeps in air, it was determined that type 5 could only operate reliably up to 70°C (Figure 62) and type 4 up to 55°C(Figure 61), which could explain why the FFT frequency does not follow the expected trend for these viscosity ranges.

To determine the sensitivity of each sensor type they were plotted over 10°C intervals starting at 30°C to 80°C. This was done by taking the FFT frequency and viscosity for each set temperature range, such as 30°C to 40°C. The change in viscosity and in FFT frequency was then calculated. This was then used to determine the sensitivity of the sensor type for that viscosity range as a change in Hertz per centistoke.

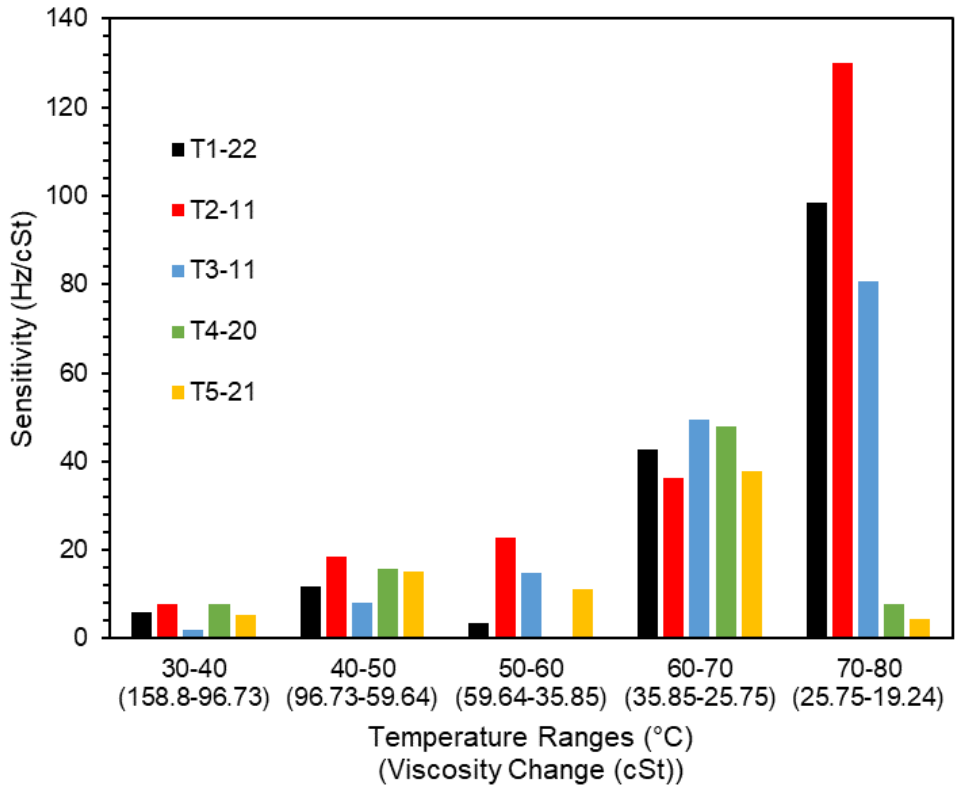

Figure 67 sensitivity of sensor types in N100 according to temperature

For the sensors in N100 they were plotted in 4 separate ranges, the slope for each sensor over the 4 ranges was then converted into change in frequency over change in viscosity. The sensitivity for each is shown in Figure 67. From the data the sensors follow a different trend than predicted. While sensors types 4 and 5 will have a larger initial displacement of the diaphragm, they are less sensitive than type 2 which has a smaller initial displacement. Type 3 is the least consistent of all the temperature ranges.

The test was then run in N35 oil to determine how the sensors react to smaller changes in viscosity. From 30°C to 80°C the viscosity of N35 changes by 39.88 cSt. The viscosity of N35 for the full temperature range 30-80°C is shown in Figure 68. Using the power trend line fitted to the data the viscosity was estimated for each temperature interval.

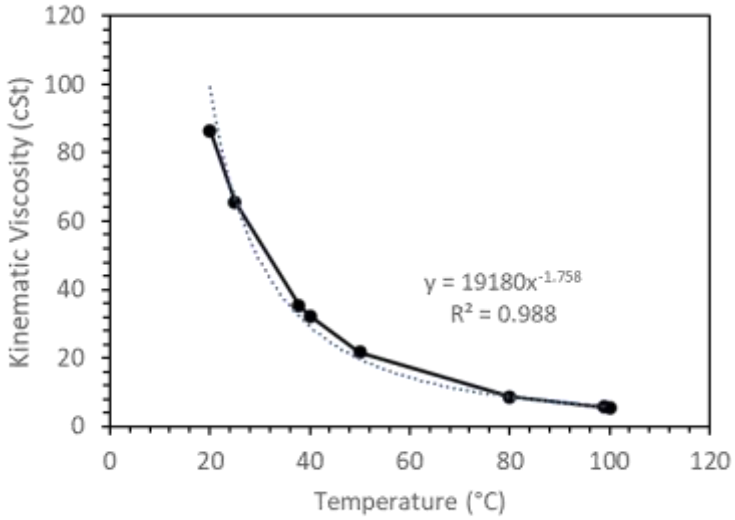

Figure 68 viscosity of N35 dependent on temperature

The results of each sensor type in N35 are shown in Figure 69. From the data Type 1 is the most accurate with an R^2 value of 0.9781.

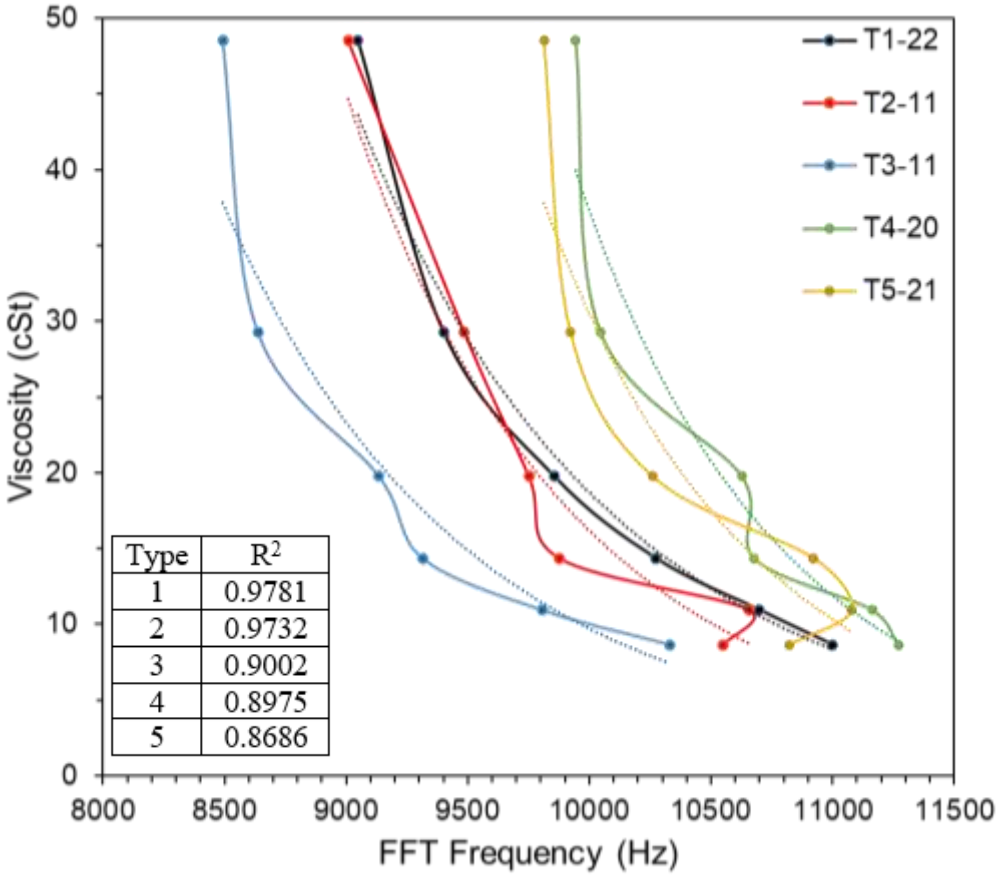

Figure 69 Sensors in N35 temperature sweep

It is followed by type 2 with an R^2 value of 0.9732. Type 5 was the least accurate with an R^2 value of 0.89. However, type 5 does not have an accurate value for 10.94-8.65 cSt range due to it being above 70°C which was determined to be the maximum operating temperature of the sensor. Type 3 had a similar in N35 as it did in N100. With an R^2 value of 0.9002 in N35 while in N100 it had a R^2 value of 0.9044.

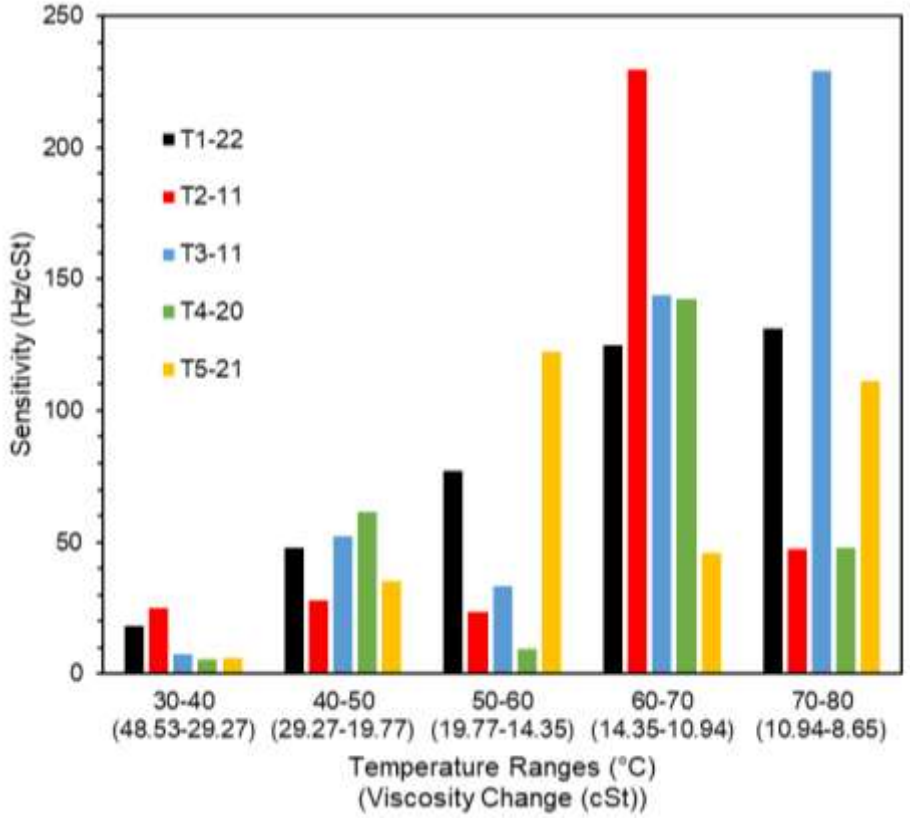

Figure 70 sensitivity of sensors in N35

To determine the sensitivity of each type over each viscosity range they were plotted together as shown in Figure 70. Type 1 had the best sensitivity across all ranges. Type 3 was the least consistent just as it was in N100.

The test was then run a final time in N10 to determine the smallest change in viscosity each sensor can detect. From 30-80°C the viscosity of N10 goes from 13.8-3.59 cSt. The viscosity values for N10 were plotted and a power trend line fitted to predict the viscosity values each temperature set point as shown in Figure 71.

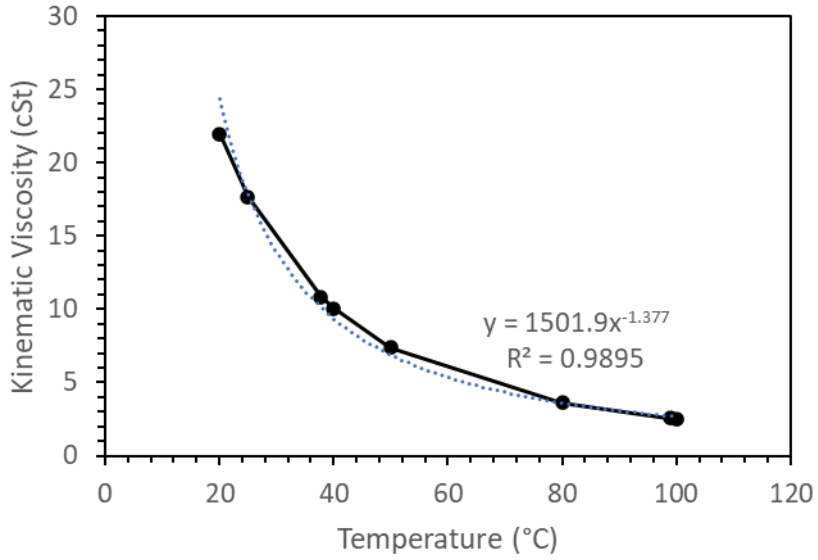

Figure 71 N10 viscosity depend on temperature.

The data from the sensors run in N10 is shown in Figure 72. From the data, type 2 is the most accurate at measuring small changes in viscosity with an R^2 value of 0.98.

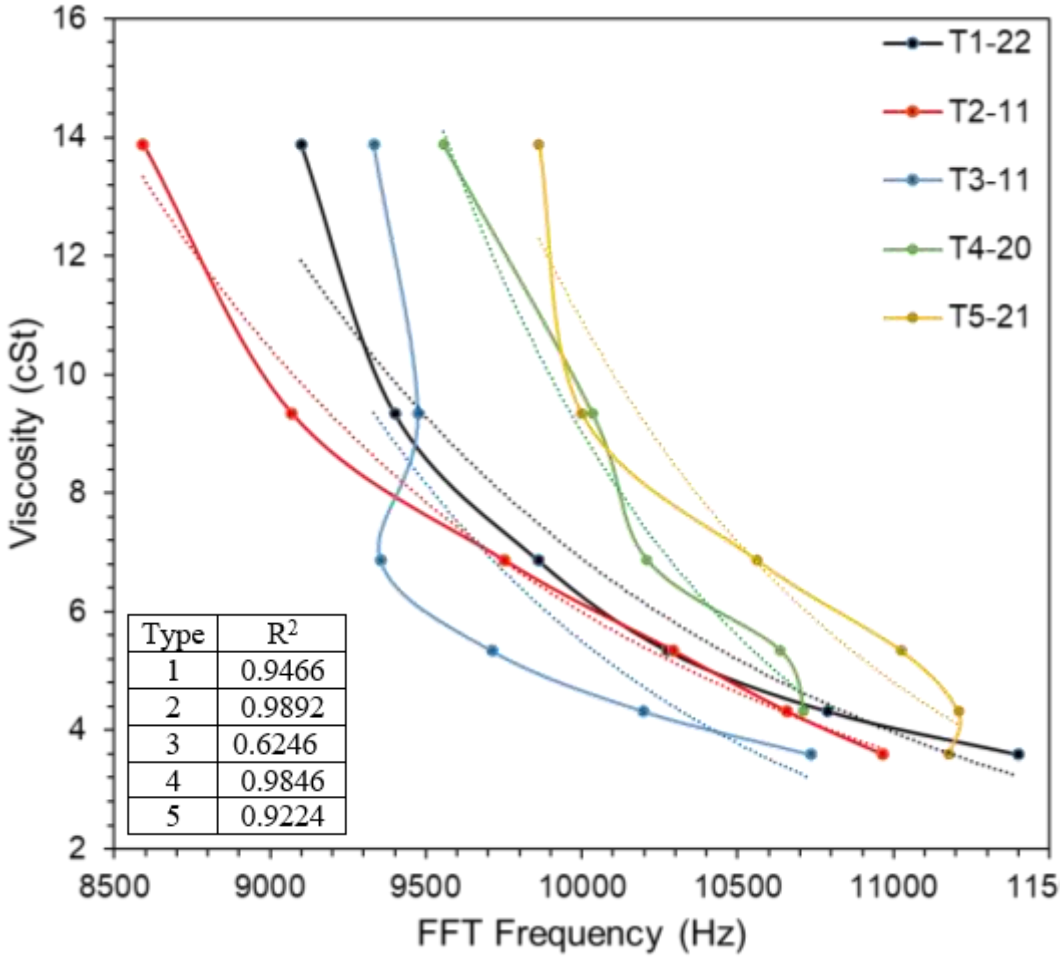

Figure 72 all sensor types in N10 temperature sweep

Because of the high R^2 value it's able to accurately measure small changes in viscosity making it the most sensitive sensor. Type 4 was the second most accurate sensor based on R^2 however type 1 appears to be more accurate.

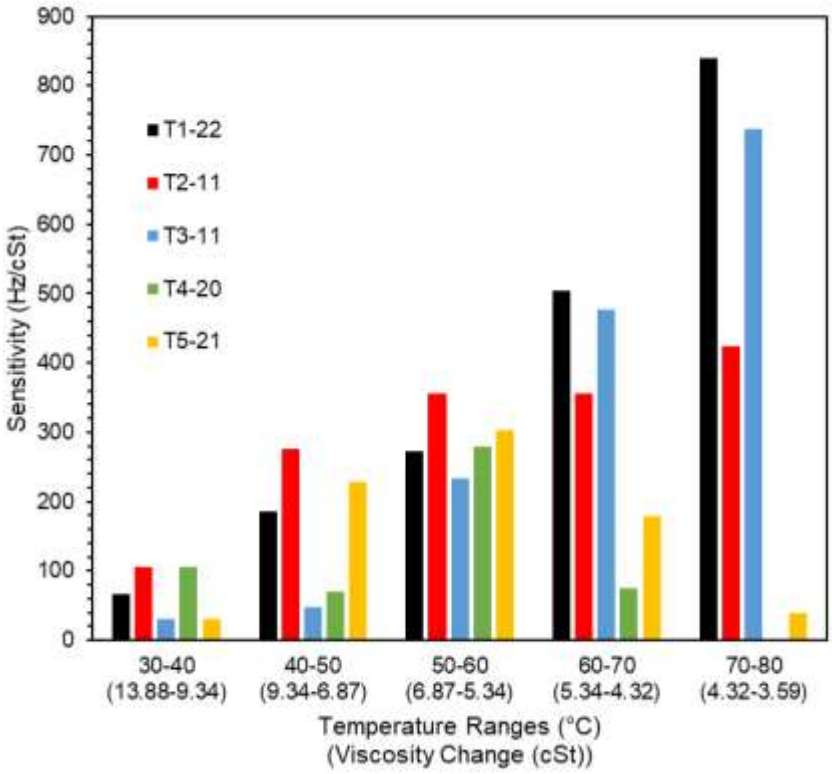

Figure 73 sensitivity of all sensor types in N10 temperature sweep

The sensitivity of each sensor was also plotted against each as shown in Figure 73. Type 1 had a higher sensitivity across all ranges followed by type 2. From the data collected from N100, N35 and N10 Types 1 and 2 are the most accurate. This goes against the original prediction that types 4 and 5 would be the most accurate since they have the largest initial deflections. From the data it actually shows that a smaller initial deflection will produce more accurate results.

Data from all of the 5 sensor types where across the standard oils sweeps where collected to determine the most arcuate sensor. This was based on the R^2 value of the power trend line fitted to each curve along with the average sensitivity of the sensor. Table 6 shows the results of the N100, N35 and N10 tests.

Oil	Starting and ending viscosity (cSt)	Viscosity range (cSt) for 30-80°C	Most accurate sensor type	R^2	Average sensitivity (Hz/cSt)
N100	158.8 to 19.24	139.56	Type 2	0.99	20.88
N35	13.88 to 8.65	39.88261932	Type 1	0.97	48.94
N10	13.8 to 3.59	10.28996414	Type 2	0.98	230.9

Table 6 Summary of Standard oil sweep

From the data Type 2 performed the best for the N100 oil with an R^2 value of 0.99 and average sensitivity of 20.88 Hz/cSt for a viscosity range of 139.56 cSt from 30-80°C. From this a change of 20.88 Hz would equate to a change of 1 cSt for this sensor. With this Type 2 will be able to detect large changes in viscosity the best.

For N35 Type 1 performed the best with a R^2 value of 0.97. The N35 oil had a total change of 39.8 cSt over the 30-80°C range and the Type 1 sensor had an average sensitivity of 48.94 Hz/cSt. This shows that Type 1 was more sensitive to smaller changes in viscosity than Type 2.

For the N10 oil Type 2 was the most sensitive for the 10.28 cSt range from 30-80°C. It had an R^2 value of 0.98 and an average sensitivity of 230.9 Hz/cSt. Due to it having the highest sensitivity Type 2 is the most accurate for small changes in viscosity being able to accurately detect changes that are below 10 cSt.

The difference in accuracy between the Type 1 and Type 2 sensor is due to the Wheatstone bridge material used. Type 2 uses P+ which produces a larger signal than the polysilicon resistors used in Type 1. Since Type 2 produces a larger signal, it is easier to detect small changes making Type 2 the most accurate.

Conclusion

5 different types of a thermally actuated MEMS viscosity sensor where successfully fabricated at RIT. Improvements to the sensor were made through the fabrication of 3 separate lots. This included better diaphragm alignment, improved uniformity of resistance across the wafers. SOI wafers were also used on the third lot to provide consistent diaphragm thickness across the wafer. These improvements allowed for a higher sensor yield that with consistent results across all types on the wafer.

Two different materials were used to create the resistors used in the Wheatstone bridge to evaluate their impact. To evaluate the Wheatstone bridge Type 1 and 2 use the same size polysilicon heater however type 1 uses polysilicon for the bridge while type 2 uses P+ resistors. Both were run in air at the same heater voltage with the same 20 Hz pulse with a width of 20 µs. The test fixture was also kept at the same gain to keep it from influencing the results. Since both types use the same heater running with the same voltage and pulse, they will have the same initial deflection. From the data collected P+ will produce an amplitude twice that of polysilicon. This shows that a P+ Wheatstone bridge will produce a larger signal allowing for more accurate viscosity measurements.

Heater material was evaluated to determine which will produce the larger temperature change to produce the largest initial deflection of the diaphragm. The purpose of having a larger initial deflection is to create a large signal that can be monitored. To properly evaluate the different heater material Type 2 and 3 used This is because they use the same P+ Wheatstone bridge and the same size heater, however they use different materials. Type 2 uses a polysilicon heater while Type 3 uses a P+ heater. Both types where also run with the same 18 V volts through the heater with a pulse of 20 Hz and width of 20 µs. From the data a polysilicon heater produces a larger deflection in air resulting in an amplitude that is approximately three times larger than the P+ heater.

To evaluate heater size three different polysilicon heaters were created to determine how the initial deflection is affected. To evaluate the effect of just the heater Types 2,4,5 and were compared since they have the same P+ Wheatstone bridge. Type 2 uses the largest heater that

1.2x1.6 mm, type 4 has the medium 0.8x1.3 mm heater while type 5 has the smallest heater that is 0.29x0.5 mm. From the data as heater size decrease the initial deflection of the diaphragm increases resulting in a larger signal amplitude. The smaller heaters can also run at lower voltages which can be useful for applications where power consumption is important. The larger amplitude is important as it can allow changes in the signal to be detected easier. However these results changed once the sensor where in oil.

From the N100, N35, and N10 temperature sweeps it was determined that larger initial deflections do not equate to a more accurate sensor. From the tests it was shown that type 2 was more accurate than types 4 and 5 which have smaller heaters (

). The second most accurate sensor was Type 1 which used the same 1.2x1.6 mm polysilicon heater as Type 2 but uses a polysilicon Wheatstone bridge. Because of the larger amplitude from the P+ Wheatstone bridge used in Type 2 it was able to have a higher sensitivity than Type 1.

Further testing will be required to determine why a larger initial amplitude actually decreases the sensitivity of the sensor. This can be done in a few ways. One method is that types 4 and 5 can be run at half the normal heater voltage, to see if decreasing the initial deflection will increase sensitivity. Another aspect to evaluate is the oil interaction with the diaphragm. With a larger displacement it could be affecting how the oil the initially couples with it. Some simulations can be created to determine how the oils interact with the diaphragm.

References

[1] A. Wolak, G. Zajac and T. Slowik, "Measuring Kinematic Viscosity of Engine Oils: A Comparison of Data Obtained from Four Different Devices," *MDPI Sensors,* vol. 21, no. 7, 2021.

[2] "Viscosity - absolute (dynamic) vs. Kinematic," [Online]. Available: https://www.engineeringtoolbox.com/dynamic-absolute-kinematic-viscosity-d_412.html. [Accessed 10 June 2023].

[3] Anton Paar, "Rotational Viscometry," [Online]. Available: https://wiki.anton-paar.com/us-en/rotational-viscometry/. [Accessed 18 June 2023].

[4] Cannon instrument company, "N100 Viscsoty standard," [Online]. Available: https://cannoninstrument.com/n100-viscosity-standard-0-5-l9727-c42-016.html. [Accessed 20 July 2023].

[5] R. Blevins, *Formulas for natrual frequency and Mode Shape,* New York: Van Nostrand Reinhold Company, 1979.

[6] Y. Kozlovsky, "Vibration of Plates in Contact with Viscous Fluid: Extension of Lamb's Model," *Journal of Sound and Vibration,* vol. 326, pp. 332-339, 2009.

[7] W. Storr, "PN junction theory for semiconductor diodes," 06 August 2022. [Online]. Available: https://www.electronics-tutorials.ws/diode/diode_2.html. [Accessed 12 June 2023].

[8] W. A. Lane and G. T. Wrixon, "The design of thin-film polysilicon resistors for analog IC applications," *IEEE Transactions on Electron Devices,* vol. 36, no. 4, pp. 738-744, 1989.

[9] D. S. Villareal, "HMDS Process," 21 Febuary 2003. [Online]. Available: https://cleanroom.utdallas.edu/manuals/hmds-process/.

[10] Brewer Science, "ProTEK B3 Coatings," [Online]. Available: https://www.brewerscience.com/products/protek-b3/. [Accessed 18 June 2023].

[11] WaferPro, "Silicon on insulator (SOI) Wafer," [Online]. Available: https://waferpro.com/silicon-on-insulator-wafers/. [Accessed 12 June 2023].

[12] I. Puchades, *MEMS Bulk Processes,* 2023.

[13] DigiKey, "IRLZ24PBF," [Online]. Available: https://www.digikey.com/en/products/detail/vishay-siliconix/IRLZ24PBF/811767. [Accessed 10 May 2023].

[14] Anton Paar, "Gravimetric Capillary Viscometer / Ubbelohde manual," [Online]. Available: https://wiki.anton-paar.com/en/gravimetric-capillary-viscometer-ubbelohde-manual/. [Accessed 18 June 2023].

Appendix A

MEMS PROCESS FLOW- Fall 2022
P+, Poly, Metal, Bottom Hole, Top Hole

	Instructions	Review/Sign
1.	Obtain qty 4, 4” n-type wafers	
2.	RCA Clean 10 min SC1, 17:1:1 H_20:H_2O_2:NH_4OH 5 min DI water rinse 60 sec 50:1 HF 5 min DI water rinse 10 min SC2 17:1:1 H_2O:H_2O_2:HCl 5 min DI water rinse SRD	
3.	Grow P+ masking oxide 6500 Å, Recipe 401 (verify) Enter Nanospec thickness:	
4.	Photo 1: P+ diffusion Coat: CEE Spin Station (HMDS, Coat MiR701 resist: 4000rpm/30sec, Softbake: 95 °C, 60sec) Expose: SUSS MA150 aligner with i-line filter and 140 sec exposure Develop: PEB: 110 °C, 60 sec, CEE Hand Developer Recipe 1 (55 sec), Hardbake: 140 °C, 60 sec) Enter minimum resolution line: _____ um	
5.	Etch Oxide ~18 min in 10:1 BOE, ER should be about 500Å/min DI water rinse SRD Verify thickness of oxide is <100Å in nanospec	
6.	Strip Resist Solvent strip/ Acetone bath/ Trion Asher (SMFL 180 sec) **Alternate:** 5 min solvent clean + 10 min DI water rinse + SRD	
7.	RCA Clean	
8.	Ion Implant B11, 1e15, 45 keV	
9.	Dopant Diffusion Recipe 341: 4000 Å wetox Soak: 20min N_2 at 1000 °C + 30min wetO_2 at 1000 °C	

	Enter Nanospec thickness: 2966 Å, 2831 Å	
10.	Four Point Probe Dummy Wafer (manual or RESMAP) Rs should be around 100 ohm/sq Voltage= _____, Current=_____ Rs: _____ ohm/sq	
11.	Deposit 1500 Å Nitride LPCVD 810C Factory Nitride recipe Soak time from log sheet= _____ Enter Nanospec thickness: 2300 Å	
12.	Coat back of wafer Photo 2: backside diaphragm Coat: CEE Spin Station (HMDS, Coat MiR701 resist: 4000rpm/30sec, Softbake: 95 °C, 60sec) Expose: SUSS MA150 aligner with i-line filter and 140 sec exposure Develop: PEB: 110 °C, 60 sec, CEE Hand Developer Recipe 1 (55 sec), Hardbake: 140 °C, 60 sec) **Note: place clean dummy-wafer on hotplate during soft/hard bakes to keep front side clean**	
13.	Spin coat resist on <u>front</u> side of wafer and protect edge Use CEE coater, S1813 resist, recipe 0 Bake at 130 °C for 1 min with pins to protect backside pattern	
14.	Etch oxynitride off backside, 1 min in 10:1 BOE	
15.	Plasma Etch Nitride on back of wafer, Lam-490 Use FACNITRIDE recipe, endpoint detection may not work due to smaller 4" wafer area. (Expect ~2'45'') Etch through nitride and SiO_2. Silicon should look cloudy/rough. Oxide left: ~ 3000 – 4000 Å W1, 2, 4: 4.5 min total (used 1st endpoint) W3: 8 min total (end point not clear)	
16.	Etch oxide (3000 Å) off backside, 8 min in 10:1 BOE	
17.	Spin coat resist on <u>back</u> side of wafer and protect edge Use CEE coater, S1813 resist, recipe 0 Bake at 130 °C for 1 min with pins to protect frontside pattern	

18.	Plasma Etch Nitride on front of wafer, Lam-490 Use FACNITRIDE recipe, endpoint detection may not work due to smaller 4" wafer area. (Expect ~2'30'') Etch through nitride and stop on SiO2.	
19.	Strip Resist Solvent strip/ Acetone bath/ Trion Asher (SMFL 180 sec) **Alternate:** 5 min solvent clean + 10 min DI water rinse + SRD	
20.	Strip resist Solvent strip 5/5 min + 5 min rinse	
21.	RCA Clean 10 min SC1, 17:1:1 H_20:H_2O_2:NH_4OH 5 min DI water rinse 60 sec 50:1 HF 5 min DI water rinse 10 min SC2 17:1:1 H_2O:H_2O_2:HCl 5 min DI water rinse SRD	
22.	Deposit 6000 Å poly LPCVD Use 610C Poly recipe Soak time from log sheet: 60 min Enter Nanospec thickness: 4700 Å – 4900 Å	
23.	Ion implant polysilicon P31, 5E15, 40 KeV	
24.	Poly Diffusion, Recipe 120 15 min in N2 at 1000C	
25.	Etch SOG 7 min 5.2:1 BOE	
26.	4 pt Probe on edge of wafer with manual 4pt probe Voltage= _____, Current=_____ Rs= _____ ohm/sq	
27.	Photo 3, Poly Coat: CEE Spin Station (HMDS, Coat MiR701 resist: 4000rpm/30sec, Softbake: 95 °C, 60sec) Expose: SUSS MA150 aligner with i-line filter and 140 sec exposure	

	Develop: PEB: 110 °C, 60 sec, CEE Hand Developer Recipe 1 (55 sec), Hardbake: 140 °C, 60 sec) Enter minimum resolution line: _____ um	
28.	Etch poly, LAM490 Use FACPOLY? recipe, endpoint detection may not work due to smaller 4" wafer area. (Expect ~1'05'') Time/wafer = 1' to 1'15''	
29.	Strip resist Solvent strip 5/5 min + 5 min rinse	
30.	RCA Clean 10 min SC1, 17:1:1 H_20:H_2O_2:NH_4OH 5 min DI water rinse 60 sec 50:1 HF 5 min DI water rinse 10 min SC2 17:1:1 H_2O:H_2O_2:HCl 5 min DI water rinse SRD	
31.	Oxidize Poly Recipe 458 Soak: 54min dryO2 at 1000C <u>Combined with Step 24</u> Enter Nanospec thickness: 1_____, 2_____, 3_____, 4_____, 5_____	
32.	Deposit 1µm TEOS TEOS in P5000 – 1um Dep time: 138 seconds Enter Nanospec thickness of bare-Si dummy wafer: 1_____, 2_____, 3_____, 4_____, 5_____	
33.	Photo 4, Contact Cut Coat: CEE Spin Station (HMDS, Coat MiR701 resist: 4000rpm/30sec, Softbake: 95 °C, 60sec) Expose: SUSS MA150 aligner with i-line filter and 140 sec exposure Develop: PEB: 110 °C, 60 sec, CEE Hand Developer Recipe 1 (55 sec), Hardbake: 140 °C, 60 sec) Enter minimum resolution line: _____ um	

34.	Etch Contact Cut in BOE, Rinse, SRD 10:1 BOE, determine etch time based on LTO thickens. Etch rate is ~1000 Å/min for TEOS and ~500 Å/min for wetox 1st etch: Enter etch time: 6.5 + 2 min 2nd etch: Enter etch time: W1,2: Enter etch time: W3, 4:	
35.	Strip resist Solvent strip 5/5 min + 5 min rinse	
36.	RCA Clean 10 min SC1, 17:1:1 H_20:H_2O_2:NH_4OH 5 min DI water rinse 60 sec 50:1 HF 5 min DI water rinse 10 min SC2 17:1:1 H_2O:H_2O_2:HCl 5 min DI water rinse 20 sec 50:1 HF 5 min DI water rinse SRD	
37.	Deposit Aluminum, 10,000 Å Glass Jar Thermal Evaporator. 4 pallets (~250 nm each) ~ 3-5 seconds pre-evaporation and open shutter Use dummy wafer with tape to measure step height. Alpha-step Al thickness = _____ Å	
38.	Photo 5, Metal Coat: CEE Spin Station (HMDS, Coat MiR701 resist: 4000rpm/30sec, Softbake: 95 °C, 60sec) Expose: SUSS MA150 aligner with i-line filter and 140 sec exposure Develop: PEB: 110 °C, 60 sec, CEE Hand Developer Recipe 1 (55 sec), Hardbake: 140 °C, 60 sec) Enter minimum resolution line: _____ um	
39.	Etch Aluminum, Wet Etch 6 min (with flat at 12 o'clock) + 1 min (with flat at 3 o'clock) Use agitation or dunking technique to ensure that Al etches in smaller spaces. Time should be 4-5 minutes.	

	Run one wafer first and inspect carefully, then the rest of wafers.	
40.	Freckle etch 1 min	
41.	Strip resist Solvent strip 5/5 min + 5 min rinse	
42.	Deposit 1µm TEOS TEOS in P5000 – 1um Dep time: 138 seconds Enter Nanospec thickness of bare-Si dummy wafer: 1_____, 2_____, 3_____, 4_____, 5_____	
43.	Photo 6, Passivation Via Coat: CEE Spin Station (HMDS, Coat MiR701 resist: 4000rpm/30sec, Softbake: 95 °C, 60sec) Expose: SUSS MA150 aligner with i-line filter and 140 sec exposure Develop: PEB: 110 °C, 60 sec, CEE Hand Developer Recipe 1 (55 sec), Hardbake: 140 °C, 60 sec) Enter minimum resolution line: _____ um	
44.	Etch LTO-TEOS Passivation 1um in Pad Etch, Rinse, SRD Get fresh pad ETCH, determine etch time based on LTO or TEOS thickens. Etch rate is ~2300Å/min???? Or dep 0.5 micron and use dry etch to open pads to Metal. Enter etch time: _____ min	
45.	Strip resist Solvent strip 5/5 min + 5 min rinse	
46.	Spin Coat PROTEK on front of wafer – See Spec Sheet Primer 1500rpm, 30sec Hot plate 140C, 30sec Coat 1500rpm, 60sec HP 140C, 120sec Oven 200C, 30min	
47.	Etch Diaphragm in KOH	

	Measure etch rate ~1.2um/min in 20062 For 270um → 225min (<4hours)	
48.	Strip PROTEK Clean	
49.	Test	